# Powered Ankle-Foot Prosthesis for the Improvement of Amputee Walking Economy

by

Samuel Kwok-Wai Au

B.Eng., Mechanical and Automation Engineering
The Chinese University of Hong Kong, 1997

M.Phil., Mechanical and Automation Engineering
The Chinese University of Hong Kong, 1999

Submitted to the Department of Mechanical Engineering
in partial fulfillment of the requirements for the degree of

Doctor of Philosophy

at the

MASSACHUSETTS INSTITUTE OF TECHNOLOGY

June 2007



Author .....
Department of Mechanical Engineering
May 4, 2007

Certified by .....
Hugh Herr
Associate Professor of Media Arts and Sciences
Assistant Professor of Health Science and Technology
Thesis Supervisor

Certified by .....
Kamal Youcef-Toumi
Professor of Mechanical Engineering
Thesis Committee Chair

Accepted by .....
Lallit Anand
Chairman, Department Committee on Graduate Students

# Powered Ankle-Foot Prosthesis for the Improvement of Amputee Walking Economy

by

Samuel Kwok-Wai Au

Submitted to the Department of Mechanical Engineering
on May 18, 2007, in partial fulfillment of the
requirements for the degree of
Doctor of Philosophy in Mechanical Engineering

## Abstract

The human ankle provides a significant amount of net positive work during the stance period of walking, especially at moderate to fast walking speeds. On the contrary, conventional ankle-foot prostheses are completely passive during stance, and consequently, cannot provide net positive work. Clinical studies indicate that transtibial amputees using conventional prostheses exhibit higher gait metabolic rates as compared to intact individuals. Researchers believe the main cause for the observed increase in metabolism is due to the inability of conventional prostheses to provide net positive work at terminal stance in walking.

This objective of this thesis is to evaluate the hypothesis that a powered ankle-foot prosthesis, capable of providing active mechanical power at terminal stance, can improve amputee metabolic walking economy compared to a conventional passive-elastic prosthesis. To test the hypothesis, a powered prosthesis is designed and buil that comprises a unidirectional spring, configured in parallel with a force-controllable actuator with series elasticity. The prosthesis is controlled to mimick human ankle walking behavior, in particular, the power generation characteristics observed in normal human walking.

The rate of oxygen consumption is measured as a determinant of metabolic rate on three unilateral transtibial amputees walking at self-selected speeds. The initial clinical evaluation shows that the powered prosthesis improves amputee metabolic economy from 7% to 20% compared to the conventional passive-elastic prostheses (Flex-Foot Ceterus and Freedom Innovations Sierra), even though the powered system is twofold heavier than the conventional devices. These results support the proposed hypothesis and also suggest a promising direction for further advancement of ankle-foot prosthesis.

Thesis Supervisor: Hugh Herr
Title: Associate Professor of Media Arts and Sciences
Assistant Professor of MIT-Harvard Division of Health Science and Technology

Thesis Committee:

Kamal Youcef-Toumi ( Committee Chairman )
Professor, Department of Mechanical Engineering

Russ Tedrake
Assistant Professor, Department of Electrical Engineering and Computer Science

Woodie C. Flowers
Professor, Department of Mechanical Engineering

# Acknowledgments

This thesis is a culmination of many people's contributions. Much of the credit for this work belongs to those listed and unlisted who donated their valuable time and thought.

I would like to thank my thesis supervisor, Professor Hugh Herr, for his advice, support, guidance and friendship during my time at the Biomechatronics Group.

I thank the members of my thesis committee: Prof. Woodie Flowers, Prof. Kamal Youcef-Toumi, and Prof. Russ Tedrake for providing invaluable insight and guidance during the preparation of this thesis.

I thank Jeff Weber, a mechanical designer in the Biomechatronics Group for designing and building different ankle prototypes for this project. The project wouldn't be such success without your help.

I also want to offer thanks to those in the Biomechatronics Group with whom I have worked for making it such an exciting working environment. Thank Waleed Farahat, Max Berniker, and Dan Paluska for being a constant source for new ideas and for feedback on existing ideas. Ernesto Martinez for his contributions to the electronics system and backpack design for the project. I also appreciate his constant support and encouragement over the past few years. Bruce Deffenbaugh for his constant willingness to help on any topic and for all the late night cups of tea. Peter Dilworth for constructing the first ankle prototype. Marko Popovic and Alice for their help in analyzing the gait data. Lee Magnusson and Chris Barnhart for their help in the metabolic cost experiment. Thanks Bob Emerson, a prosthetist from Next Step O&P, for getting the patients and helping in the clinical study. Thank you to every one who agreed to participate in the study. Thanks to all of them and to everyone else who has worked in the research group.

Besides, I thank some of the members of the dArbeloff Lab, including Eric Wade, Kyu-Jin Cho, and Philip Shaltis for their support and help in my first two years at MIT. In particular, Eric Wade, thank you for being so patient with me in the past six years when I was learning to survive at MIT and never making me feel badly about asking so many questions.

I thank all of the members in the Hong Kong Bible Study Group at MIT for providing an excellent community for me that was supportive, friendly, and constructive for my growth in Christ.

I thank my parents, my brothers, and sisters for their continuous support and encouragement.

I thank my love, Joan Chan for her constant love and for the happiness she has brought to my life.

Finally, I want to thank my lord, Jesus Christ for giving me a chance to study at MIT and helping me to survive in the graduate school in the past six years. Also bring me a new life and new purpose. This thesis is dedicated to him.

# Contents

# List of Figures

# List of Tables

# Chapter 1

# Introduction

Today's commercially available below-knee prostheses are completely passive during stance, and consequently, their mechanical properties remain fixed with walking speed and terrain. These prostheses typically comprise elastic bumper springs or carbon composite leaf springs that store and release energy during the stance period, e.g. the Flex-Foot or the Seattle-Lite [1][2].

Lower extremity amputees using these conventional passive prostheses experience many problems during locomotion. For example, transtibial amputees expend 20-30% more metabolic power to walk at the same speed than able-bodied individuals, and therefore, they prefer a slower walking speed to travel the same distance. Thus, their self-selected walking speed is normally 30-40% lower than the mean speed of intact individuals [3][4]. Also, many clinical studies report that amputees exhibit an asymmetrical gait pattern [6][7][8]. For example, unilateral below-knee amputees generally have higher than normal hip extension, knee flexion, and ankle dorsiflexion on the unaffected side. On the affected side, such individuals have less than normal hip and knee flexion during stance. Additionally, there is a significant ankle power difference between the affected and unaffected sides during ankle powered plantar flexion in walking.

There are many differences between the mechanical behavior of conventional ankle-foot prostheses during the walking cycle and that of the human ankle-foot complex. Most notably, the human ankle performs more positive mechanical work than negative, especially at moderate to fast walking speeds [10]-[15]. Researchers hypothesize that the primary source of energy loss in walking is to "pay" for the redirection of the center of mass velocity during step-to-step transitions [17][18][19]. Researchers have shown that supplying energy through the ankle joint to redirect the center of mass is more economical than to exert power through the hip joint alone [17][19]. These biomechanical results may explain why transtibial amputees require more metabolic energy to walk than intact individuals. Using a conventional passive prosthesis, a leg amputee can only supply energy through the hip joint to power center of mass dynamics, producing a pathological gait pattern [6][7][8].

In this thesis, it is hypothesized that the inability of conventional passive prostheses to provide net positive work over the stance period is the main cause for the aforementioned clinical problems. The goal of this thesis is to evaluate the hypothesis

through development of a physical prototype of a powered ankle-foot prosthesis[1] to demonstrate its benefits to a transtibial amputee ambulation.

## 1.1 State-of-the-Art

Although the idea of a powered ankle-foot prosthesis has been discussed since the late 1990s, only one attempt has been made to develop such a prosthesis to improve the locomotion of amputees. Klute [20] attempted to use an artificial pneumatic muscle, called McKibben actuator to develop a powered ankle-foot prosthesis. Although the mechanism was built, no further publications have demonstrated its capacity to improve amputee gait compared to conventional passive-elastic prostheses.

More recent work has focused on the development of quasi-passive ankle-foot prostheses [21][22][23]. Collins and Kuo [21] advanced a foot system that stores elastic energy during early stance, and then delays the release of that energy until late stance, in an attempt to reduce impact losses of the adjacent leg. Since the device did not include an actuator to actively plantar flex the ankle, no net work was performed throughout stance. Other researchers [22][23] have built prostheses that use active damping or clutch mechanisms to allow ankle angle adjustment under the force of gravity or the amputee's own weight.

In the commercial sector, the most advanced ankle-foot prosthesis, the Össur Proprio Foot$^{TM}$ [1], has an electric motor to adjust foot position during the swing phase to achieve foot clearance during level-ground walking. Although active during the swing phase, the Proprio ankle joint is locked during stance, and therefore becomes equivalent to a passive spring foot. Consequently, the mechanism cannot provide net positive power to the amputee.

## 1.2 Engineering Challenges

According to [6][9][26], two main engineering challenges hinder the development of a powered ankle-foot prosthesis.

- *Mechanical design*
  With current actuator technology, it is challenging to build an ankle-foot prosthesis that matches the size and weight of the human ankle, but still provides a sufficiently large instantaneous power and torque output to propel an amputee. For example, a 75 kg person has an ankle-foot weight of approximately 2.5 kg, and the peak power and torque output at the ankle during walking at 1.7 m/s can be up to 350 W and 150 Nm, respectively [10][12][9]. Current ankle-foot mechanisms for humanoid robots are not appropriate for this application, as they are either too heavy or not powerful enough to meet the human-like specifications required for a prosthesis [27][28].

[1] In this thesis, a powered ankle-foot prosthesis is defined as an ankle-foot prosthesis that can provide sufficient net positive work during the stance period of walking to propel an amputee.

- *Control system design*
  A powered prosthesis must be position and impedance controllable. Often robotic ankle controllers follow pre-planned kinematic trajectories during walking [27][28], whereas the human ankle is believed to operate in impedance control mode during stance and position control mode during swing [11][12]. Furthermore, for the ease of use, only local sensing for the prosthesis is preferable, which adds extra constraints on the control system design. Finally, there is no clear control target or "gold standard" for the prosthesis to be controlled, against which to gauge the effectiveness. It is unclear what kind of prosthetic control strategy is effective for the improvement of amputee ambulation.

## 1.3 Research Objective

The objective of this thesis is to evaluate the following hypothesis: a powered ankle-foot prosthesis improves transtibial ambulation, in particular the walking economy. In this thesis, improving walking economy means decreasing the metabolic cost of transport (COT), which is defined as the metabolic energy spent per unit body weight per unit distance [24].

To meet this objective, this thesis comprises three research components:

- the advancement of a powered ankle-foot prosthesis to allow different prosthetic control systems to be evaluated on transtibial amputees;
- the development of a control system for the powered prosthesis that mimics normal human stance period dynamics;
- a clinical evaluation of the powered prosthesis on three unilateral transtibial amputees walking on level-ground surfaces.

## 1.4 Thesis Outline

In Chapter 2, I review the human ankle biomechanics in walking.

In Chapter 3, I propose a stance phase control scheme of the prosthesis that mimicks the quasi-static stiffness behavior and power generation characteristics of the human ankle during steady state walking, called target stance phase behavior. I hypothesize that using this target stance phase behavior in an ankle-foot prosthesis may reduce a transtibial amputee walking economy.

In Chapter 4, I specify the design specifications for the prosthesis based on the human ankle walking biomechanics. I present a novel motorized prosthesis, called MIT Powered Ankle-Foot Prosthesis, that exploits both series and parallel elasticity with an actuator to fulfill the demanding human-like ankle specifications. I first describe the basic configuration and a minimal model for the powered ankle-foot prosthesis.

I propose several design analyses to guide the selection of system components. Finally, I describe the physical embodiment of the proposed prosthesis and present the experimental results for the system characterization.

In Chapter 5, I present a control system architecture that allows the prosthesis to provide the target stance phase behavior. It includes the design of low-level controllers and a finite-state controller that utilizes low-level controllers to mimic the normal human ankle behavior during the stance period of walking.

In Chapter 6, I present details of the clinical evaluation on three unilateral transtibial amputees, which includes experimental protocols and the clinical results. The clinical study consists of three sessions: Basic Clinical Gait Study , Metabolic Cost Study, and Kinematics and Kinetics Study. I discuss the results at the end of this chapter.

In Chapter 7, I outline the contributions of this thesis and propose future avenues of investigation.

# Chapter 2

# Background

Understanding normal walking biomechanics provides the basis for the design and control of the powered prosthesis. In this chapter, I first review biomechanics of normal human ankle-foot for level-ground walking. I then present an overview of conventional ankle-foot prostheses. Finally, I dicuss typical locomotion problems experienced by the transtibial amputees using conventional prostheses.

## 2.1 Normal Human Ankle-Foot Walking Biomechanics

Walking is a highly coordinated behavior accomplished by intricate interaction of the musculo-skeletal system. Researchers have spent many efforts to understand the corresponding principle for human walking [29][24][10][25][31][30]. Preliminary introduction to human walking can be obtained through Inman [24] and Perry [25]. Winter [10][32][33] also provides a detailed analysis of kinematic, kinetic and muscle activation patterns of human gait.

This chapter focuses on providing the basic concepts of human walking, in particular, the function of human ankle in the sagittal plane during level-ground walking. Along the lines of the research in [11]-[14][25], the function of the human ankle is characterized in terms of simple mechanical elements, rather than using a complex biomechanical model. Such simple functional models motivate and simplify the design and control of the powered prosthesis. They also provide a means by which the performance of any artificial ankle could be measured against that of a biological ankle [11].

### 2.1.1 Normal Gait

A level-ground walking gait cycle is typically defined as beginning with the heel strike of one foot and ending at the next heel strike of the same foot [24][25]. The main subdivisions of the gait cycle are the stance phase (about 60% of a gait cycle) and the swing phase (about 40% of a cycle)(Fig. 2-1). The swing phase (SW) represents

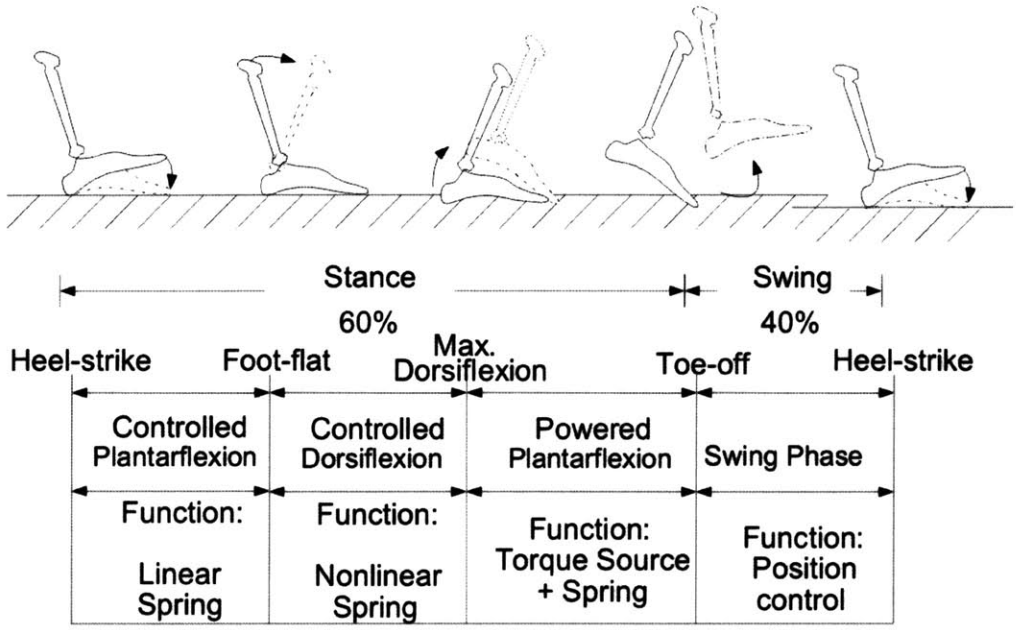


Figure 2-1: Normal human ankle biomechanics for level-ground walking.

the portion of the gait cycle when the foot is off the ground. The stance phase begins at heel-strike when the heel touches the floor and ends at toe-off when the same foot rises from the ground surface. From [11][12], the stance phase of walking can be divided into three sub-phases: Controlled Plantar Flexion (CP), Controlled Dorsiflexion (CD), and Powered Plantar Flexion (PP). These phases of gait are described in Fig. 2-1. In addition, Fig. 2-2 shows the typical ankle torque-angle characteristics for a 75kg person walking at a self-selected speed (1.25m/sec). The detailed descriptions for each sub-phase are provided below.

*Controlled Plantar Flexion (CP)*

CP begins at heel-strike and ends at foot-flat. Simply speaking, CP describes the process by which the heel and forefoot initially make contact with the ground. In [11][12][25], researchers showed that ankle joint behavior during CP is consistent with a linear spring response with joint torque proportional to joint position. As can be seen in Fig. 2-2, segment (1)-(2) illustrates the linear spring behavior of the ankle.

*Controlled Dorsiflexion (CD)*

CD begins at foot-flat and continues until the ankle reaches a state of maximum dorsiflexion. Ankle torque versus position during the CD period can often be described as a nonlinear spring where stiffness increases with increasing ankle position. The main function of the human ankle during CD is to store the elastic energy necessary to propel the body upwards and forwards during the PP phase [11]-[15]. Segment (2)-(3) in Fig. 2-2 reveals the nonlinear spring behavior of the human ankle joint dur-

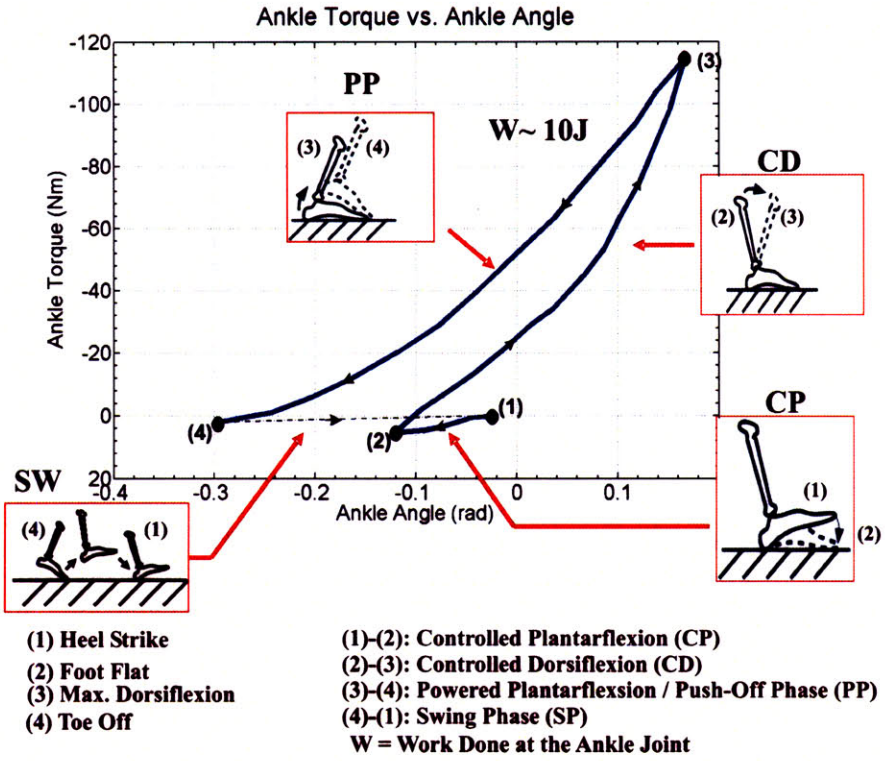


Figure 2-2: A typical ankle torque-angle behaviour for a 75 kg person at a self-selected walking speed(1.25m/sec). Data are from [12], re-plotted in the manner of [26]. The solid line shows the ankle torque-angle behaviour during stance while the dash line shows the ankle behaviour during the swing phase. The points (1),(2),(3), and (4) represent the conditions of the foot at heel-strike, foot flat, maximum dorsiflexion, and toe-off, respectively. The segments (1)-(2), (2)-(3), (3)-(4), and (4)-(1) represent the ankle torque-angle behaviours during CP, CD, PP, and SW phases of gait, respectively. As can be seen in (a), segments (1)-(2) and (2)-(3) reveals the different spring behaviors of the human ankle during CP and CD, respectively. The area W enclosed by points (2), (3), and (4) is the net work done at the joint.

ing CD.

*Powered Plantar Flexion (PP)*

PP begins after CD and ends at the instant of toe-off. Because the work generated during PP is more than the negative work absorbed during the CP and CD phases for moderate to fast walking speeds [10]-[15], additional energy is supplied along with the spring energy stored during the CD phase to achieve the high plantar flexion power during late stance. Therefore, during PP, the ankle can be modeled as a torque source in parallel with the CD spring. The area $W$ enclosed by the points (2), (3), and (4) shows the amount net work done at the ankle.

*Swing Phase (SW)*

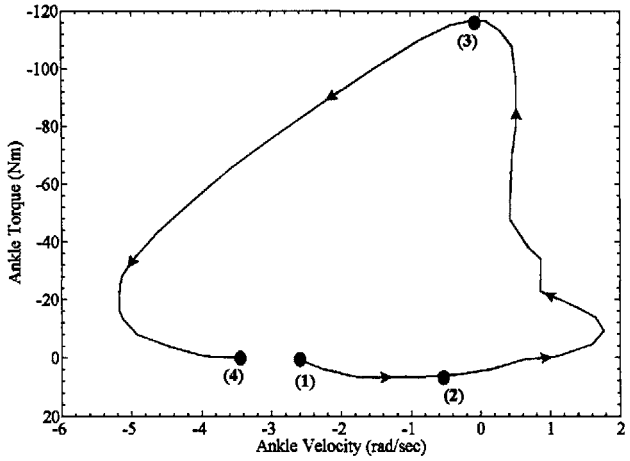


Figure 2-3: A typical ankle torque-velocity behaviour for a 75 kg person at a self-selected walking speed(1.25m/sec). The points (1),(2),(3), and (4) represent the conditions of the foot at heel-strike, foot flat, maximum dorsiflexion, and toe-off, respectively.

SW begins at toe-off and ends at heel-strike. It represents the portion of the gait cycle when the foot is off the ground. During SW, the ankle can be modeled as a position source to reset the foot to a desired equilibrium position before the next heel strike.

In summary, for level ground walking, human ankle provides three main functions: (i) it behaves as a spring with variable stiffness from CP to CD;(ii) it provides additional energy for push-off during PP; and (iii) it behaves as a position source to control the foot orientation during SW.

### 2.1.2 Ankle-Foot Biomechanics Versus Walking Speed

In the literature [10][11][12], normal human ankle does more net positive work as the walking speed increases. As revealed in Fig. 2-4, the net work done at the ankle joint is approximately zero for slow walking speed. This suggests that the normal human ankle can be modeled as a spring at slow walking speed (0.9 m/s). Approaching the fast walking speed ( 1.8 m/s), there is a dramatic increase in the quasi-static stiffness[1] of human ankle from CD to early PP, consequently, more net positive work has done at the ankle joint. This phenomenon motivates us to model the ankle behavior as a combination of a spring component and a constant offset torque source during PP. Details of the model description will be discussed in Chapter 3.

Besides, it is shown that there is a lower bound (or offset value) in the quasi-static stiffness from CD to PP for all walking speeds (Fig. 2-4(a)). This also motivates the design of using a physical spring, configured in parallel to the joint of the powered

[1]Quasi-static stiffness is the slope of the measured ankle torque-angle curve of the human ankle during walking.

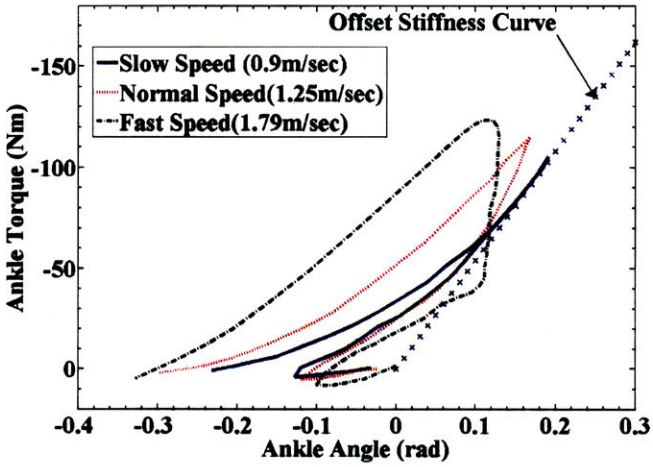


(a) Ankle Torque vs. Ankle Angle

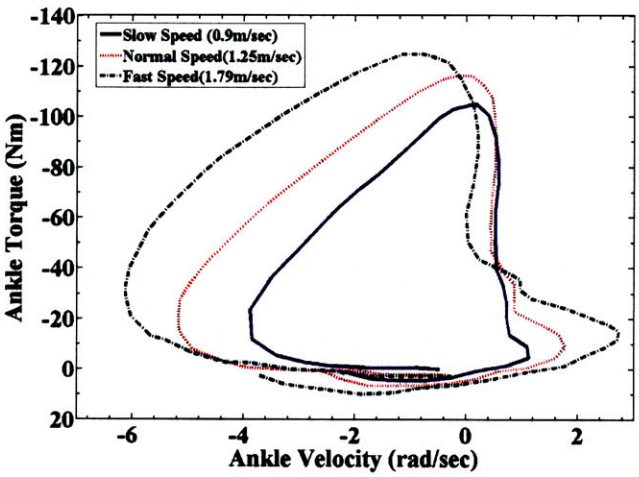


(b) Ankle Torque vs. Ankle Velocity

Figure 2-4: Ankle torque-angle/velocity behavior for different walking speeds [12]. As can be seen in (a), Normal human ankle behaves as a spring for slow walking speed. However, it does more net positive work as the walking speed increases.

(a) SACH foot (b) Flex-foot (c) Proprio Foot$^{TM}$

Figure 2-5: Examples of conventional ankle-foot prostheses. (Photos Courtesy of Össur, inc. and ING, Corp.)

prosthesis to provide the offset stiffness.

## 2.2 Conventional Ankle-Foot Prostheses

Conventional ankle-foot prostheses used by lower limb amputees can be divided into two main categories: nonenergy-storing feet and energy-storing feet (or dynamic elastic response feet). A typical example of the nonenergy-storing feet is the Solid Ankle, Cushioned Heel (SACH) foot (Fig. 2-5(a)) [2]. The SACH foot is composed of a rigid longitudinal keel with a solid ankle. A wedge of polyurethane foam provides cushioning in the heel section, with hyperextension of the rubber toe section possible during late stance. It was designed with the goal of restoring basic walking and simple occupational tasks and was once considered as the optimum compromise between durability and functional effectiveness, as well as being of reasonable cost in the early 80's [2].

Energy-storing feet were introduced in the late 80's due to the incorporation of modern lightweight, elastic materials into the design of ankle-foot prostheses. These prostheses were designed to deform during heel contact and mid-stance and rebound during late stance to simulate the "push-off" characteristics of a normal ankle. They were designed for very active unilateral or bilateral transtibial amputees to foster springy walking, running and jumping but may be used by all lower-limb amputees [2]. The Össur's Flex-foot (Fig. 2-5(b)) [1] is an icon of such kind of prostheses.

The most advanced ankle-foot prosthesis, the Össur's Proprio Foot$^{TM}$(Fig. 2-5(c)) [1], has an electric motor to adjust the orientation of a low profile Flex-foot during the swing phase. As its ankle joint is locked during stance, the prosthesis behaves equivalent to a typical energy-storing feet during the stance period of walking.

Whatever, conventional ankle-foot prostheses can only partially restore the functions of a biological ankle-foot described in Section 2.1. A brief summary of functional comparison between a biological ankle-foot and conventional prostheses is shown below based on the results from [2][10][11][12].

- Normal human ankle has a larger range of movement than conventional passive-elastics prostheses.

- Normal human ankle stiffness varies within each gait cycle and also with walking speed. Although most conventional prostheses are designed to have stiffness variations within a gait cycle, these stiffness variations are limited and are only designed for a particular walking speed.

- Normal human ankle provides a significant amount of net positive work during the stance period of level-ground walking, stair ascent, and slope climbing. The conventional prostheses, including the Proprio Foot$^{TM}$, cannot provide any net positive work during stance.

- Normal human ankle behaves as a rotary damper during the early stance of stair descent to absorb a significant amount of impact energies/power [12]. Due to the passive-elastic nature, most of conventional prostheses cannot absorb/dissipate such a large amount of energy during stair descent. Consequently, during stair descent, amputees need to place their prostheses on each step gently to minimize the impact and also use either their knee or hip joints to dissipate the extra energy [69][68].

## 2.3 Transtibial Amputee Gait

The gait of transtibial (or below-knee (B/K)) amputee subjects has been extensively studied by means of kinematics and kinetics analysis, as well as energy cost techniques [6][7][8]. Results from these studies indicates that the transtibial amputee gait demonstrates a distinct different from the gait of an able-individual. This section focuses on the gait of unilateral transtibial amputees using the conventional passive-elastic ankle-foot prostheses. The following shows the common observations in amputee gait, compared to normal gait:

- The average B/K amputee's self-selected speed (0.97 m/s) is slower than mean normal (1.3 m/s) [6].

- Average stride length of an B/K amputee is slightly shorter, as compared to the mean normal [6].

- There is a distinct asymmetry in B/K amputees' gait.

  - The range of ankle movement on the affected side (or prosthetic side) is smaller or limited, compared to that of the unaffected side [7][8].
  - Hip extension moment on the affected side from early to mid-stance is greater than normal, that results in above-normal energy generation by the hip joint on the affected side. It is believed that this extra amount of energy is used to partially compensate the lack of active push-off in the prostheses [6][8].

  - Due to the above-normal hip extension, the knee flexion moment on the affected side during early stance is below the mean normal value. Consequently, the power generated by the knee joint during the early stance are near zero [6][8].
  - There is a significant ankle power difference between the affected and unaffected sides during ankle powered plantar flexion in walking [6][7][8].

- Transtibial amputees are known to spend greater amounts of energy while walking than non-amputees do [3][4][5]. The magnitude of disparity appears to be dependent on the cause of amputation [37][40]. Young adult traumatic amputee, while expending energy at a 25 percent greater rate than normal walking, accomplished only 87 percent of the normal velocity. Due to lack the necessary physiological vigor and strength, dysvascular amputees expended energy at a 38 percent greater rate than normal walking, while only accomplished 45 percent of the normal velocity.

All the differences in the gait can be attributed to an attempt by the amputee to compensate for the missing prosthetic ankle-power generation by producing more power at the hip.

Besides, researchers also conducted experiments to study the effect of different ankle-foot prostheses, including the nonenergy-storing and energy-storing feet on amputee gait [7][34][36][35]. Although most amputee subjects comment that energy-storing feet are better than the non-energy-storing one, results from these studies indicate that there is no significant difference in amputee gait associated with these two kinds of prosthetic feet (e.g. SACH foot vs. Flex-foot ). Although [39] has shown that traumatic amputee's walking metabolic cost can be slightly improved when using energy-storing feet, in general, there is also no significant differences in amputee walking metabolic cost associated with these feet [38][37],

# Chapter 3

# Desired Ankle Behavior

Regarding the control issues of the powered ankle-foot prosthesis, there is no clear control target or "gold standard" for the prosthesis to be controlled, against which to gauge the effectiveness. In this chapter, I propose a stance phase control scheme that mimicks the quasi-static stiffness behavior and power generation characteristics of the human ankle during steady state walking, called target stance phase behavior. I hypothesize that an ankle-foot prosthesis using this control scheme increases a transtibial amputee walking economy.

## 3.1 Target Stance Phase Behavior

Referring to Section 1.2, the key question for the control is to define a target walking behavior for the prosthesis. For the swing phase, the desired ankle behavior is just to re-position the foot to a predefined equilibrium position. For the stance phase control, instead of simply tracking ankle kinematics, researchers [11][12][14] suggest that one simple way is to let the prosthesis mimic the "quasi-static stiffness", that is the slope of the measured ankle torque-angle curve during stance. This quasi-static stiffness curve describes the energy (net work) flow characteristics between the human ankle and the environment during steady state walking.

In this thesis, the main goal of the stance phase control for the powered prosthesis is to mimic the quasi-static stiffness curve, so as to deliver net positive work to an amputee. Using the biomechanical descriptions in [11][12], the quasi-static stiffness curve (Fig. 3-1(A)) can be decomposed into two main components: (i) a spring whose stiffness varies in a similar manner as the normal human ankle does in CP and CD; (ii) a torque source that provides positive net work during late stance phase. The torque source is assumed to be active between points (4) and (3). Such a functional decomposition allows us to study the effect of performing net positive work during stance on amputee ambulation independent of the stiffness variation.

For the ease of experimentation and clinical evaluation, I simplify and parameterize these two components and used them to provide the target stance phase behavior for the prosthesis as depicted in Fig. 3-1B. Detailed descriptions for each component are summarized as follows:

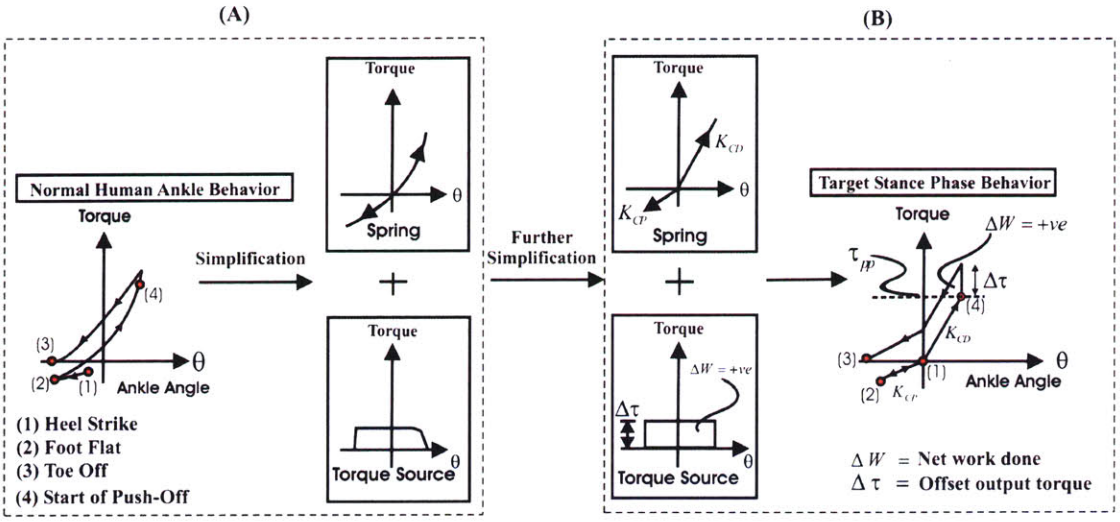


Figure 3-1: Target stance phase behavior. The normal human ankle behavior (quasi-static stiffness curve) was decomposed into a spring component and a torque source. The spring component was then piecewise linearized and its stiffness varies with the sign of the ankle angle. The torque source was modeled as a constant offset torque $\Delta\tau$, which was applied to the ankle joint from points (4) to (3).

1. A torsional spring with a stiffness $K_{ankle}$ that varies with the sign of the ankle angle $\theta$ as follows.

$$K_{ankle} = \begin{cases} \mathrm{K}_{CP} & \theta \leq 0 \\ \mathrm{K}_{CD} & \theta > 0 \end{cases} \tag{3.1}$$

   When the ankle angle is positive, the stiffness value will be set to $K_{CD}$. When the ankle angle is negative, the stiffness value will be set to $K_{CP}$.

2. A constant offset torque $\Delta\tau$ that models the torque source during PP. This offset torque will be applied in addition to the torsional spring $K_{CD}$ during PP. The torque threshold $\tau_{pp}$ determines the moment at which the offset torque is applied, indicated by the point (4) in Fig. 3-1B. The total work done $\Delta W$ at the ankle joint by the torque source is

$$\Delta W = \Delta\tau(\frac{\tau_{pp}}{K_{CD}} + \frac{\Delta\tau}{K_{CP}}) \tag{3.2}$$

   The $\frac{\tau_{pp}}{K_{CD}}$ indicates the starting ankle angle at which the torque source is applied while $\frac{\Delta\tau}{K_{CP}}$ represents the stopping ankle angle at which the control system stop applying the torque source to the ankle joint.

Using the stance phase control scheme (Fig. 3-1B), one can conduct experiment to study the clinical effect of a particular parameter value (e.g. $K_{CP}$) to amputee

ambulation. In particular, the control scheme facilitates the study of the clinical effect of performing the net positive work to amputee ambulation because the amount of net positive work performed at the ankle joint can be controlled based on Eqn. (3.2). It is noted that the conventional passive prostheses only provide the spring behavior but fail to supply the function of the torque source to thrust the body upwards and forwards during PP. Our designed prosthesis eventually will provide both functions during stance. I hypothesize that an ankle-foot prosthesis that can provide the target stance phase behavior may improve a transtibial amputee walking economy.

# Chapter 4

# Mechanical Design and Analysis

In this chapter, I present a novel, motorized ankle-foot prosthesis, called MIT Powered Ankle-Foot Prosthesis. This prosthesis exploits both series and parallel elasticity with an actuator to fulfil the demanding human-ankle specifications. I begin this chapter by describing the design specifications of a powered ankle-foot prosthesis. I then present the overall design architecture of the proposed prosthesis. I propose several design analyses to guide the selection of system components. Finally, I describe the physical embodiment of the prosthesis and present the experimental results for the system characterization.

## 4.1 Design Specifications

Using the biomechanical descriptions in Section 2.1 and the results from [11][12][24], the design goals for the prosthesis are summarized as follows:

- the prosthesis should be at a weight and height similar to the intact limb.
- the system must deliver a large instantaneous output power and torque during push-off.
- the system must be capable of changing its stiffness as dictated by the quasi-static stiffness of an intact ankle.
- the system must be capable of controlling joint position during the swing phase.
- the prosthesis must provide sufficient shock tolerance to prevent damage to the mechanism during the heel-strike.

It is important to note that the prosthesis and controller designs are not independent. Rather, they are integrated to ensure that the inherent prosthesis dynamics do not inhibit controller's ability to specify desired dynamics. This topic is discussed further in Section 4.4. In the remainder of this section, the target parameters for the design goals are outlined.

- *Size and Weight:*
  The height of normal human ankle-foot-shank complex (measured from the ground to the knee joint) is about 50 cm for a 75 kg person with a total height of 175 cm [25]. In average, the level of amputations for a transtibial amputee is about two third of the length of normal human ankle-foot-shank complex, which is about 32 cm [2]. A rough estimation of the weight of the missing limb for that given height is around 2.5 kg. In fact, it is favorable to minimize the height of prosthesis because the shorter the length of a prosthesis is, the more amputees can fit to it.

- *Range of Joint Rotation:*
  The proposed range of joint rotation for the prosthesis is based on normal human ankle range of motion during walking [24]. The maximum plantarflexion (20-25 degrees) occurs just as the foot is lifted off the ground, while the maximum dorsiflexion (10-15 degrees) happens during CD.

- *Torque and Speed:*
  According to [11][12], the measured peak velocity, torque, and power of the human ankle during the stance period of walking can be as high as 5.2 rad/s, 140 Nm, and 350 W, respectively (Fig. 2-3). Rather than just satisfying the peak conditions, the maximum torque-speed characteristic of the prosthesis is designed to bracket that of the human ankle during walking.

- *Torque Bandwidth:*
  The torque bandwidth is computed based on the power spectrum of the nominal ankle torque data for one gait cycle. In this thesis, the torque bandwidth is defined at the frequency range over which covers 70% of the total power of the signal. Analyzing the normal human ankle data in [12], the torque bandwidth was found to be about 3.5 Hz in which the ankle torque varies between 50 to 140 Nm. The goal is to design a torque/force controller whose bandwidth is larger than the specified torque bandwidth (3.5 Hz). More specifically, this controller should be able to output any torque level between 50 - 140 Nm at 3.5 Hz. It implicitly suggests that the large force bandwidth of the open-loop system need to be much larger than 3.5 Hz, otherwise, the inherent prosthesis dynamics may inhibit controller's ability to specify desired dynamics.

- *Net Positive Work:*
  In the literature, the average values of the net positive work done at the ankle joint for medium and fast walking speeds of a 75 kg person are about 10 J and 20 J, respectively [11][12].

- *Offset Stiffness:*
  The offset stiffness during CD is obtained by computing the average slope of the measured human ankle torque-angle curve of the human ankle during CD [11][12]. The mean value of the offset stiffness is about 550 Nm/rad and is applicable to a large range of walking speed from 1 m/s to 1.8 m/s.

A summary of the parameters values of the above design goals are provided in Table 4.1.

Table 4.1: Design Specifications

| | |
|---|---|
| Weight (kg) | 2.5 |
| Max. Allowable Dorsiflexion (deg) | 15 |
| Max. Allowable Plantarflexion (deg) | 25 |
| Peak Torque (Nm) | 140 |
| Peak Velocity (rad/s) | 5.2 |
| Peak Power (W) | 350 |
| Torque Bandwidth (Hz) | 3.5 |
| Net Work Done (J) | 10J at 1.3m/s |
| Offset Stiffness During CD (Nm/rad) | 550 |

## 4.2 Overall Mechanical Design

It is challenging to build an ankle-foot prosthesis that matches the size and weight of an intact ankle, but still provides a sufficiently large instantaneous power output and torque for the powered plantarflexion [6][9]. Typical design approaches [27][28] that use a small-sized actuator along with a high gear-ratio transmission to actuate ankle-foot mechanism may not be sufficient to overcome these design challenges for the two reasons. First, due to the high transmission ratio, this approach may have difficulty in generating a large instantaneous output power because the effective motor inertia has significantly increase by $N^2$, where $N$ is the gearing reduction ratio. Second, the large reduction ratio also reduces the system's tolerance to the impact load. During walking, there is a substantial amount of impact load applying on the prosthesis during the heel-strike. This may cause damage to the transmission.

My design approach is to use a parallel spring with a force-controllable actuator with series elasticity to actuate an ankle-foot mechanism. The parallel spring and the force-controllable actuator serve as the spring component and the torque source in Fig. 3-1B, respectively. The prosthetic ankle-foot system requires a high mechanical power output as well as a large peak torque. The parallel spring shares the payload with the force-controllable actuator, thus the required peak force from the actuator system is significantly reduced. Consequently, a smaller transmission ratio can be used, and a larger force bandwidth is obtained. The series elasticity is also an important design feature for the ankle-foot prosthesis as it can prevent damage to the transmission due to shock loads, especially at heel-strike.

The basic architecture of the mechanical design is shown in Fig. 4-1. As can be seen, there are five main mechanical elements in the system: a high power output d.c. motor, a transmission, a series spring, a unidirectional parallel spring, and a carbon composite leaf spring prosthetic foot. The first three components are combined to form a force-controllable actuator, called Series-Elastic Actuator(SEA). A SEA, previously developed for legged robots [41][42], consists of a dc motor in series with a

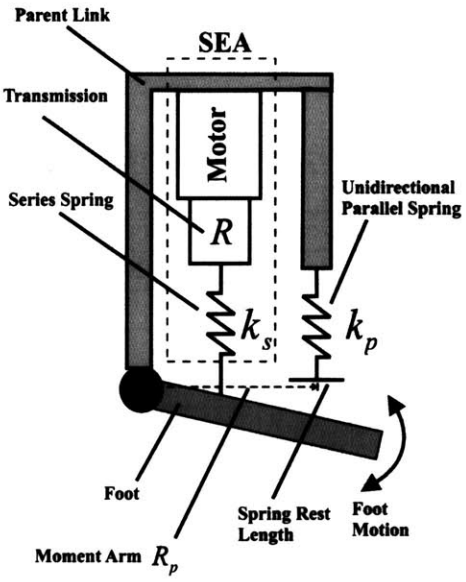


Figure 4-1: Schematics of the powered ankle-foot prosthesis.

spring (or spring structure) via a mechanical transmission. The SEA provides force control by controlling the extent to which the series spring is compressed. Using a linear potentiometer, we can obtain the force applied to the load by measuring the deflection of the series spring.

In this application, I use the SEA to modulate the joint stiffness as well as provide the constant offset torque $\Delta\tau$. As can be seen in Fig. 4-2, the SEA provides a stiffness value $K_{CP}$ during CP and a stiffness value $K_{CD1}$ from CD to PP. From points (4) to (3), it supplies both the stiffness value $K_{CD1}$ and a constant, offset torque $\Delta\tau$.

Due to the demanding output torque and power requirements, I incorporate a physical spring, configured in parallel to the SEA, so that the load borne by the SEA is greatly reduced. Because of the reduced load, the SEA will have a substantially large force bandwidth to provide the active push-off during PP. To avoid hindering the foot motion during swing phase, the parallel spring is implemented as an unidirectional spring that provides an offset rotational stiffness value $K_p^r$ only when the ankle angle is larger than zero degree (Fig. 4-2).

To further understand the benefits of the parallel spring, a simulation was conducted to illustrate the effect of the parallel spring to the reduction of the actuator output torque and power. In the simulation, kinematics of the normal human ankle (Fig. 4-3a) was applied to the prosthesis depicted in Fig. 4-1, while the prosthesis were required to output a similar torque and power profiles as the normal human ankle does for a gait cycle. Assuming that the force-controllable actuator (SEA) in the prosthesis is a perfect torque source and is able to output any given torque trajectory. If there is no parallel spring, the actuator output torque and power behavior have to be the same as the that of normal human ankle. When the stiffness of the parallel spring was increased, the actuator output torque and power were significantly

reduced. (Fig. 4-3). For example, in the simulation, the required peak actuator output power ( 174 W) with $K_p^r = 300$ rad/s was about 35% less than the case ( 265 W) without the parallel spring. Furthermore, with that parallel spring, the peak output torque was reduced from 118Nm to 60Nm. In addition, the positive work done by the actuator was reduced from 18.3 J to 11.8 J. Although increasing the parallel spring stiffness can substantially reduce the actuator peak output torque and power, the stiffness of the parallel spring should not be set above the nominal offset stiffness. If the parallel spring is too stiff for the amputee user, the force controllable actuator may need to provide negative stiffness to compensate the excess stiffness of the parallel spring.

The elastic leaf spring foot is used to emulate the function of a human foot that provides shock absorption during foot strike, energy storage during the early stance period, and energy return in the late stance period. A standard prosthetic foot, Flex Foot LP Vari-Flex [1] is used in the prototype.

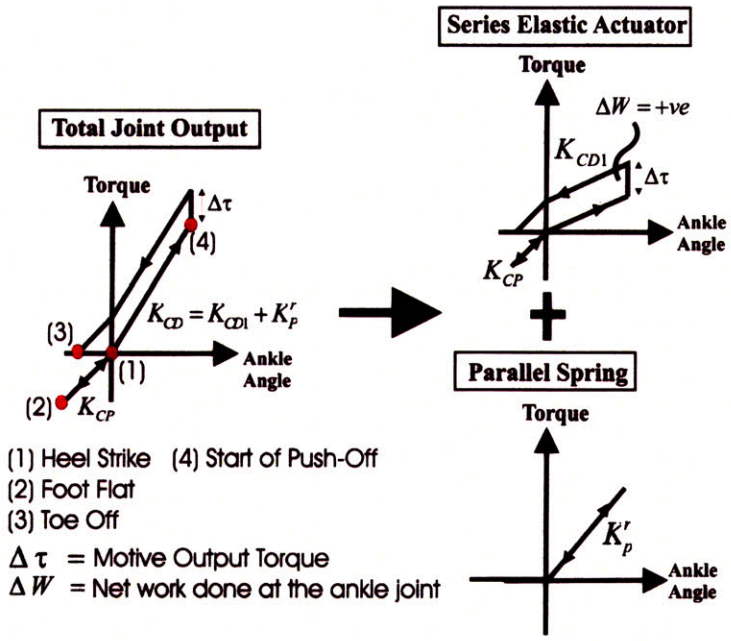


Figure 4-2: Exploiting the parallel and series elasticity with an actuator. The parallel spring provides a biased, offset stiffness $K_p^r$ when the ankle angle is larger than zero degree. The series spring combined with the actuator, called an SEA [41][42], is used to modulate the joint stiffness and serve as a torque source for performing positive work at the ankle joint.

## 4.3 System Model

A linear model is proposed in Fig. 4-4 that is sufficient to describe the essential linear behavior of the prosthesis. The model is adopted from the standard SEA

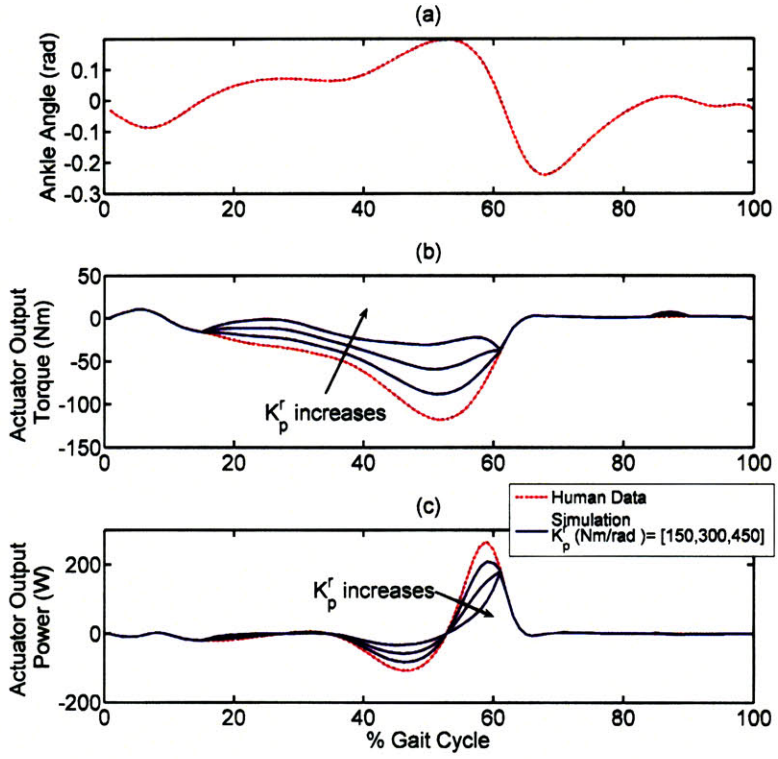


Figure 4-3: Simulation of the required actuator output torque and power for different parallel springs. The human gait data is from [12]

model [42], except that I apply his model to a rotational joint system and also include a unidirectional parallel spring into the model. Referring to the Fig. 4-4(a), the motor is modeled as a torque source $T_m$ with a rotary internal inertia $I_m$, applying a force to the series spring $k_s$ through a transmission $R$. The damping term $b_m$ represents the brush and bearing friction acting on the motor. $x$ and $\theta$ are the linear displacement of the series spring and the angular displacement of the ankle joint, respectively.

In this model, we assume the foot is a rigid body with negligible inertia because it is relatively very small compared to the effective motor inertia, i.e., $T_{ext} = rF_s$ where $T_{ext}$ and $r$ are the moment arm of the spring about the ankle joint and the torque exerted by the environment to the prosthesis. This model ignores the amplifier dynamics, nonlinear friction, internal resonances, and other complexities.

For simplicity, we then convert the model into translational domain (see Fig. 4-4(b)). $M_e$, $B_e$, and $F_e$ represent the effective mass, damping, and linear force acting on effective mass, respectively. These components are defined as follows: $M_e = I_m R^2$, $F_e = T_m R$, $B_e = B_m R$. The equation of motion becomes:

$$M_e\ddot{x} + B_e\dot{x} = F_e + F_s \tag{4.1}$$

$$F_s = k_s(r\theta - x) \tag{4.2}$$

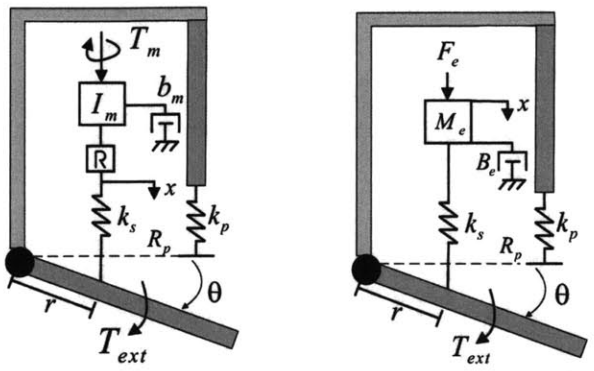


(a) Rotational Domain

(b) Translational Domain

Figure 4-4: Linear models for the prosthesis. (a) rotary domain (b) translational domain.

while the total external torque or total joint torque

$$T_{ext} = \begin{cases} \mathrm{rF}_s & \theta < 0 \\ \mathrm{rF}_s + R_p k_p \theta & \theta \geq 0 \end{cases} \tag{4.3}$$

Eqns. (4.1) and (4.2) are the standard dynamic equations for a SEA [42]. Eqn. (4.3) reveals that with the parallel spring, less spring force $F_s$ is required for a given total joint torque. This model will be used to guide the design and control analysis in the rest of the thesis.

## 4.4 Design Analysis

In this section, both steady-state and dynamic design analyses are proposed to guide the design of the powered prosthesis. These analyses focus on designing the prosthesis to satisfy the torque-speed characteristic and torque bandwidth requirement specified in Section 4.1. The steady-state analysis assists in designing the maximum torque-speed characteristic of the prosthesis to bracket that of the human ankle during walking. The dynamic analyses guides us to select the system components (e.g. series spring) to maximize the prosthesis output acceleration and meet the torque bandwidth requirement. The details of the analyses are described as follows.

### 4.4.1 Steady-State Analysis for Design

The purpose of the steady-state analysis provides a calculation on the maximum torque/power-speed characteristic of the prosthesis. This help us select the actuator and transmission for the prosthesis such that its maximum torque/power-speed characteristics can match with that of an intact ankle(Fig. 2-3). In this analysis, as I am only interested in the effect of the actuator saturation and transmission ratio to the maximum torque-speed characteristic, thus the effect of the parallel spring,

series spring, and the frictional loss in the brush motor are not taken into account in this analysis. The actuator and transmission selection will then be verified using the dynamic analysis discussed in Section 4.4.2. With this assumption, the ankle joint torque becomes $T_{ext} = rRT_m$. Because motors have limits to the instantaneous torque and velocity output capabilities, a motor's performance is generally bounded by

$$T_m(\omega) \leq T_m^{max} - \omega(\frac{T_m^{max}}{\omega^{max}}) \tag{4.4}$$

where $T_m, \omega, T_m^{max}, \omega^{max}$ are the motor torque, motor velocity, motor stall torque, and maximum motor velocity, respectively. Let $R_{total} = rR$ be the total transmission ratio of the system. Then the torque-speed characteristics of the prosthesis is bounded by

$$T_{ext}(\dot{\theta}) \leq R_{total}T_m^{max} - R_{total}\dot{\theta}(\frac{T_m^{max}}{\omega^{max}}) \tag{4.5}$$

If we define a torque trajectory $T_h(\dot{\theta})$ that represents the normal human ankle torque-speed characteristic as shown in Fig. 2-3, the design goal is to have $T_{ext}(\dot{\theta})$ always greater than $T_h(\dot{\theta})$ for any given velocity or

$$T_h(\dot{\theta}) < T_{ext}(\dot{\theta}) \qquad \forall\dot{\theta} \tag{4.6}$$

$$\leq R_{total}T_m^{max} - R_{total}\dot{\theta}(\frac{T_m^{max}}{\omega^{max}}) \qquad \forall\dot{\theta} \tag{4.7}$$

Eqn. (4.7) demonstrates the primary design goal of the prosthesis, i.e., the selection of the motor $(T_m^{max}, \omega^{max})$ and transmission $(R_{total})$ for the prosthesis should always satisfy Eqn. (4.7). Practically, there are many other engineering factors that may reduce the maximum torque output of the actual prototype such as frictional loss, stiction, current saturation of motor amplifier, and geometry of the transmission, it is favorable to have the maximum output torque at least two times larger than the required one. Fig. 4-5 shows a simulation of the maximum torque/power-speed characteristics of the prosthesis with different total transmission ratios. In the simulation, a d.c. brush motor from Maxon, Inc with a part number RE-40 was used. Its stall torque and the maximum angular velocity of the motor are up to 2.5 Nm and 7580 rpm, respectively. To fulfil Eqn. (4.7), we used a transmission ratio $R \sim 3560$ and moment arm $r$ =0.0375 m, i.e. $R_{total} = 133$. As indicated in Fig. 4-5(a), the contour of the maximum torque profile of the designed prosthesis was always larger than that of the normal human ankle. Furthermore, the power output characteristics of the prosthesis was designed to match with that of the intact ankle during walking, where they both output peak power around 3 rad/s. It was also found that the maximum allowable transmission ratio is about 142. Eqn. (4.7) will not be satisfied for any $R_{total}$ larger than 142 for the given motor.

### 4.4.2 Dynamic Analysis for Design

Satisfying the torque/power-speed constraint in the steady-state analysis is the basic design requirement for the prosthesis. However, it does not guarantee that the pros-

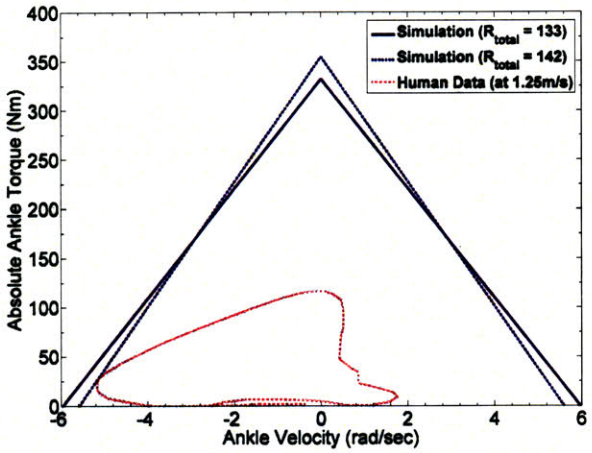


(a) Absolute Joint Torque vs. Joint Velocity

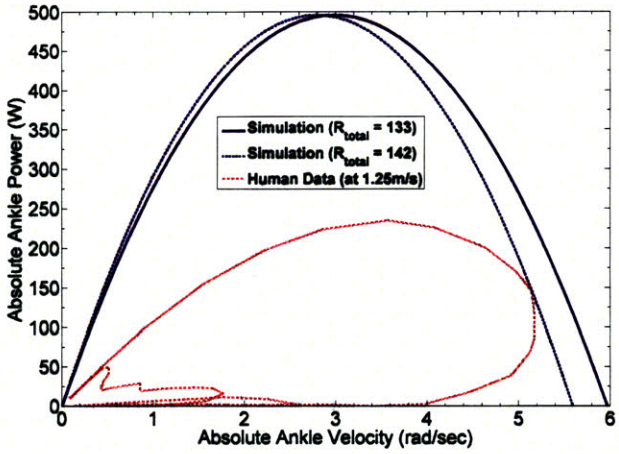


(b) Absolute Joint Power vs. Absolute Joint Velocity

Figure 4-5: Comparisons of the maximum joint torque/power-speed characteristic of the prosthesis to that of the normal human ankle during walking.

thesis is actually capable of mimicking the normal ankle behaviors in the dynamic condition. In this section, I study the system output acceleration and its relationship to the choice of the transmission ratio and parallel spring. I also look at the output force bandwidth of the prosthesis in the consideration of motor saturation.

### System Output Acceleration

The primary performance measure for a powered ankle-foot prosthesis is determined by how fast the prosthesis can output a constant offset torque $\Delta\tau$ to an amputee user during PP. The key to maximizing the step response performance is to maximize the system output acceleration. According to [49][51], there are two basic principles of maximizing the system output acceleration for a given load: (a) If the source inertia is adjustable, the source inertia should be minimized; (b) For a given source inertia, select a transmission ratio such that the input and output impedance of the system

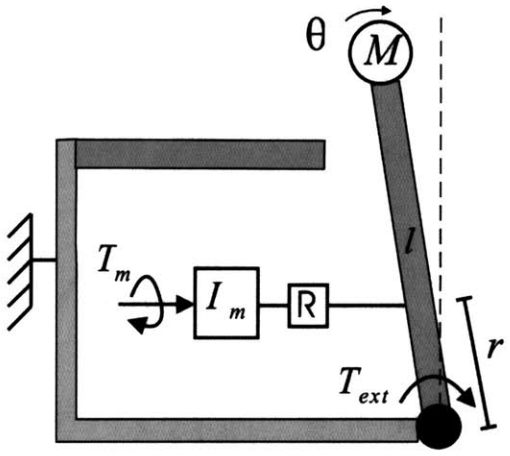


Figure 4-6: A model to study the system output acceleration. This model represents the prosthesis driving a fixed load mass $M$.

can be matched. However, in practice, motors always have a finite inertia which is not adjustable. Thus, in general, the second approach is normally used to maximize the the system output acceleration in machine design.

To obtain the intuition, I start with the model shown in Fig. 4-6. This model represents the prosthesis driving a fixed load mass $M$. My interest is to obtain insights into the effect of the load mass and the transmission ratio to the output acceleration for a given actuator torque and internal inertia. The effect of the parallel, series elasticity, the frictional loss in the system will be considered later in this section.

The dynamic equation of this model can be written as

$$\ddot{\theta} = \frac{T_m R_{total}}{Ml^2 + I_m R_{total}^2} \tag{4.8}$$

where $R_{total} = rR$. Differentiating Eqn. (4.8) with respect to $R_{total}$ gives the optimal transmission ratio

$$R_{opt} = \sqrt{\frac{Ml^2}{I_m}} \tag{4.9}$$

The maximum output joint acceleration $\ddot{\theta}_{max}$ for a given actuator effort is

$$\ddot{\theta}_{max} = \frac{T_m}{2\sqrt{I_m M}} \tag{4.10}$$

Fig. 4-7 shows the system output acceleration of various transmission ratios and load masses. In this simulation, I set the motor inertia $I_m$=134 g-cm$^2$ and load mass from 25-75 kg. Using the optimal transmission ratio does not guarantee that the system can fulfill the torque-speed constraints specified in Eqn. (4.7). It is noted that for a given motor inertia, the optimal transmission ratio is always larger than the allowable transmission ratio ($R_{total} = 142$) obtained in Section 4.4.1.

According to [51], adding the frictional loss or damping term into the model will

only lower the peak acceleration, but not significantly change the overall relationship between the transmission ratio and the output acceleration for a given actuator effort as shown in Fig. 4-7.

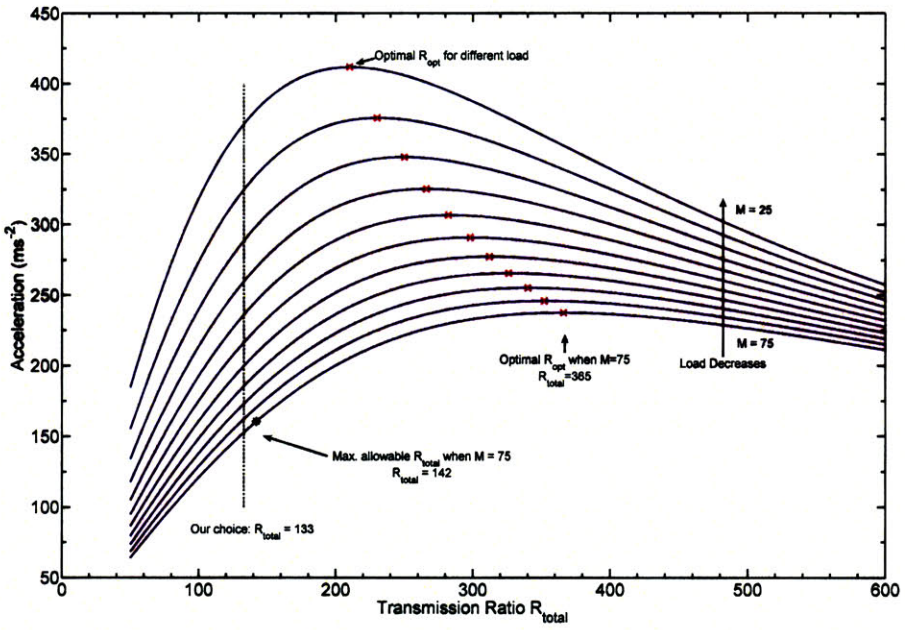


Figure 4-7: System output acceleration of various transmission ratio and load mass. The system always outputs the maximum acceleration at the optimal transmission ratios for the corresponding load masses. The red cross indicates the optimal transmission ratio for a given load mass.

The effect of the model with parallel elasticity can be described using the model in Fig. 4-8. Consider the case when the motor drives the load mass forward while the unidirectional spring has been preloaded by an angle $\theta_o$. The instantaneous system acceleration can then be written as

$$\ddot{\theta} = \frac{T_m R_{total} + K_p R_p \theta_o}{Ml^2 + I_m R_{total}^2} \tag{4.11}$$

. Besides the term $K_p R_p \theta_o$ due to the parallel spring, Eqn. (4.11) is exactly the same as Eqn. (4.8). This term allows the system to output the acceleration with less actuator effort. In other words, the system can generate higher peak acceleration for a given actuator effort. In addition, differentiating Eqn. (4.11) w.r.t $R_{total}$ will give us the same optimal transmission ratio as described in Eqn. (4.9).

Until now, I have not discussed how the series spring will affect the dynamic behavior of the system. Generally speaking, adding a series spring degrades performance properties of the prosthesis such as the system output acceleration and system bandwidth [42]. In the next section, I will provide some basic principles that guide us to select the series spring, satisfying the desired dynamic requirements.

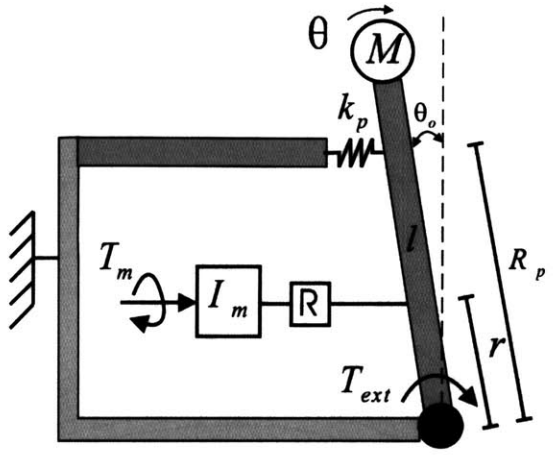


Figure 4-8: A model to study the system output acceleration with the unidirectional spring.

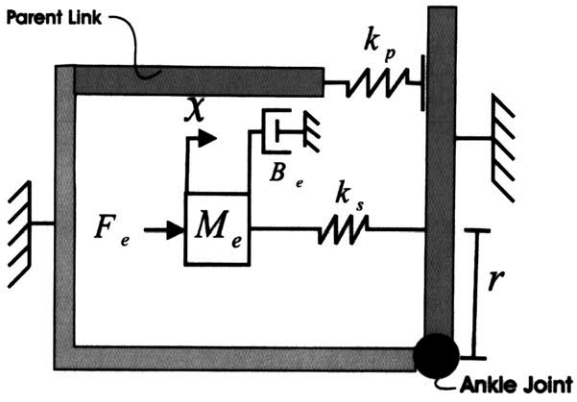


Figure 4-9: System bandwidth analysis. Both ends of the prosthesis are fixed to the ground. The parallel spring will not be engaged in this condition.

### Large Force Bandwidth of the System

Before designing any controllers for a SEA, we need to guarantee that the system will not run into any saturation or system limitation within the operating range of the torque level and bandwidth. One suggested index to measure the limitation of the system's dynamic performance is the "large force bandwidth" [42]. Large force bandwidth is defined as the frequency range over which the actuator can oscillate at a force amplitude $F_s^{max}$ due to the maximum input motor force, $F_{sat}$ [42]. The series elasticity substantially reduces the system bandwidth at large force due to motor saturation. The stiffer the spring is, the higher SEA bandwidth is at large force. The design goal is to select a proper series spring $k_s$ such that the large force bandwidth of the SEA is much greater than the required force bandwidth in Table 4.1.

To study the large force bandwidth, both ends of the prosthesis are fixed (see Fig. 4-9), consequently, the parallel spring does not affect the dynamic of the system.

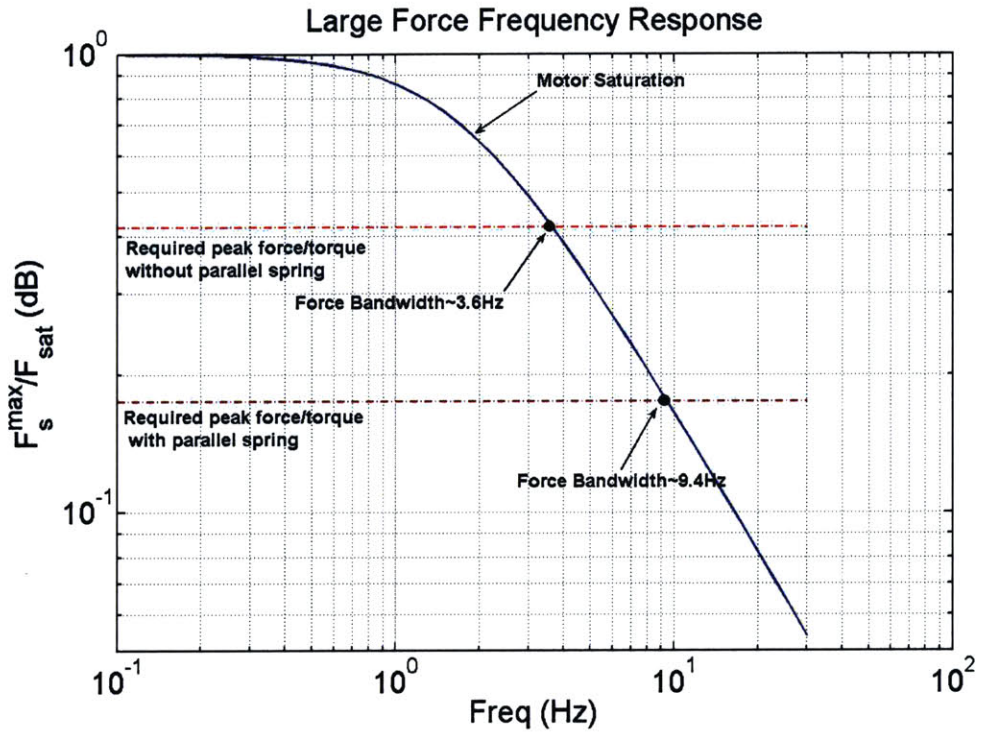


Figure 4-10: Simulation result for the large force bandwidth due to motor saturation.

The spring force $F_s$ is considered as the system output. This system is a standard SEA with fixed end condition [42]. The transfer function $G_{fixed}(s)$ between the input $F_e$ and output force $F_s$ of the system is defined as:

$$G_{fixed}(s) = \frac{F_s}{F_e} = \frac{k_s}{M_e s^2 + B_e s + k_s} \tag{4.12}$$

The effect of motor saturation can be thought of as a input motor force $F_{sat}$ in parallel with a damper of a appropriate damping ratio $B_{sat} = \frac{F_{sat}}{V_{sat}}$, where $F_{sat}$, $V_{sat}$ are the maximum motor force and velocity due to the motor saturation, respectively. They are defined as $F_{sat} = RT_{motor}^{max}$ and $V_{sat} = \frac{\omega^{max}}{R}$. Incorporating the damping term $B_{sat}$ into the Eqn. (4.12), the transfer function that describes the large force bandwidth is:

$$\frac{F_s^{max}}{F_{sat}} = \frac{k_s}{M_e s^2 + (B_e + \frac{F_{sat}}{V_{sat}})s + k_s} \tag{4.13}$$

where $F_s^{max}$ is the maximum output force. As can be seen in Eqn. (4.13), the large force bandwidth is independent of the control system, but depends on the intrinsic system dynamics that are determined by the choices of the motor, transmission ratio, and the spring constant.

Fig. 4-10 graphically shows the large force bandwidth of the system. In the simulation, $k_s$ was set to be 1200 kN/m, while the same motor parameters and transmission ratio were used as in Section 4.4.1. The corresponding model parameters for

Table 4.2: Model Parameters

| Parameters | $F_{sat}$ | $V_{sat}$ | $M_e$ | $B_e$ |
|---|---|---|---|---|
| Values | $7654N$ | $0.23m/s$ | $170kg$ | $8250Ns/m$ |

Eqn. (4.13) were computed and are shown in Table 5.1. The value of the frictional loss $B_e$ was based on a measurement from the actual prototype (see Section 4.5.2).

As shown in Fig. 4-10, the estimated large force bandwidth of the system without the parallel spring is 3.6 Hz at 120 Nm, which is slightly larger than the required force bandwidth of the system (3.5 Hz). Note that the lower the required force, the larger the force bandwidth.

Although this simulation only described the output force bandwidth for a fixed-end condition, it can also provide some insights into the effect of the parallel spring on the system bandwidth. According to Eqn. (4.3), the parallel spring shared some of the payloads of the SEA, and the required peak force for the system was significantly reduced. For example, given $R_p$= 0.0375 m,$k_p$=380 rad/s, $\theta$ = 10 rad, $T_{ext}$=120Nm, the required peak torque for the SEA is only 50 Nm, and the estimated force bandwidth (9.4 Hz) becomes almost three times larger than the designed one. In practice, it is favorable to design a system whose large force bandwidth is several times larger than the required bandwidth as there are many factors that can substantially reduce the large force bandwidth, such as unmodeled friction.

Fig. 4-11 shows the step response of the prosthesis at $F_e = F_{sat}$. Due to the velocity saturation of the motor, the system response is highly over-damped. The settling time of the step response is about 0.2 seconds.

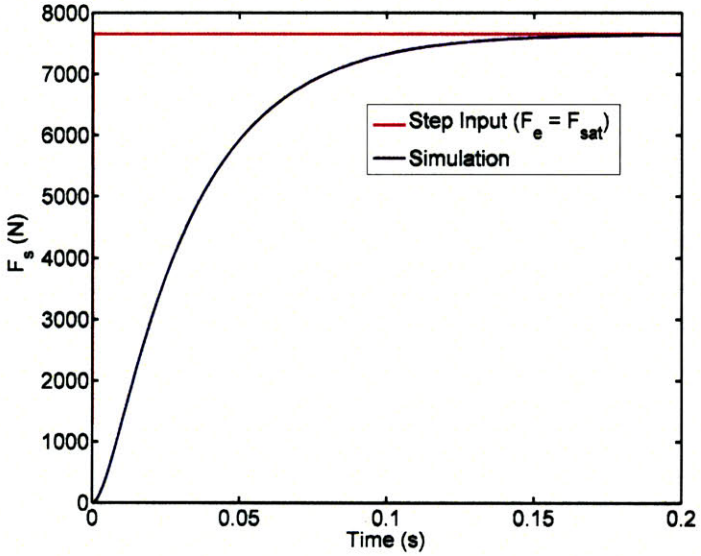


Figure 4-11: Simulation result for the step response at $F_e = F_{sat}$. The system response is highly over-damped due to the motor saturation

### 4.4.3 Design Procedure

Below is some suggested procedures/guidelines on the design of the prosthesis.

1. Select a motor and transmission ratio that can fulfil the steady-state requirements in Section 4.4.1.

2. Check the system output acceleration using the suggested motor and transmission ratio using the analysis in Section 4.4.2. Make sure that the suggested motor and transmission can provide sufficient system output acceleration, otherwise re-do step (1).

3. Select the series spring stiffness that have a large force bandwidth larger than the required one in Table 4.1, otherwise re-do step (1) and (2).

## 4.5 Physical Embodiment

The physical prototype of the prosthesis was developed in collaboration with a mechanical designer, Jeff Weber of the Biomechatronics Group. My work was on the design of the system architecture and component selections while he focused on the CAD design. The physical prototype was fabricated by a machine shop outside the lab. Figs. 4-12, 4-13 and 4-14 show the CAD Model, images, and the schematics of the actual prototype, respectively. I also compared the specifications for the current design and the design specifications in Table 4.3. The current design specifications were estimated based on the system components and the simulation results in Section 4.5.1.

Table 4.3: A summary of the specifications for the current design

| | Desired Value | Current Design |
|---|---|---|
| Weight (kg) | 2.5 | 2.9 |
| Length (m) | N/A | 0.3 |
| Max. Allowable Dorsiflexion (deg) | 15 | 20 |
| Max. Allowable Plantar flexion (deg) | 25 | 25 |
| Peak Torque (Nm) | 140 | 330 |
| Peak Velocity (rad/s) | 5.2 | 6 |
| Peak Power (W) | 350 | 500 |
| Torque Bandwidth (Hz) | 3.5 | 9 |
| Offset Stiffness (Nm/rad) | 550 | 380 |

### 4.5.1 Component Selection and Implementation

#### Actuator and Transmission

The first step in the design is to select an actuator and a transmission to satisfy the torque/power-speed requirements of the human ankle (Fig. 4-5). In the design,

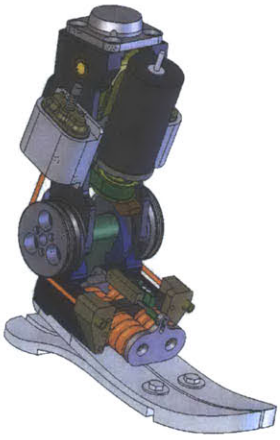

(a) Front View

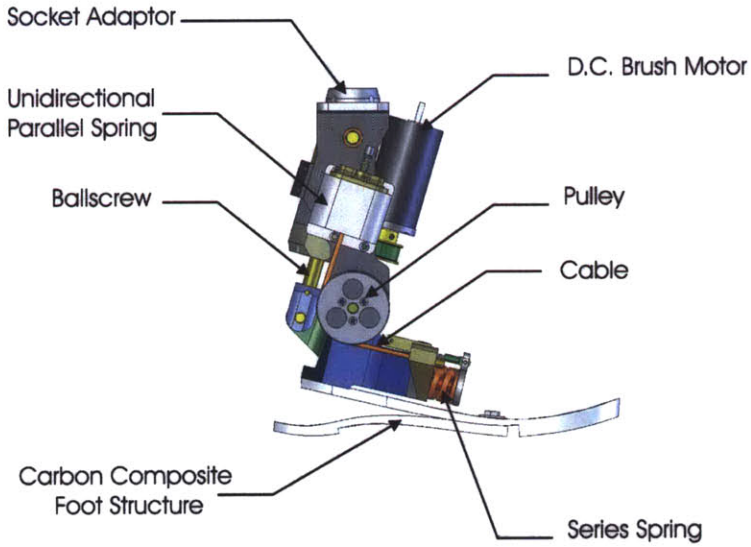


(b) Side View

Figure 4-12: Mechanical design of the prosthesis.

a 150 W d.c. brushed motor from Maxon, Inc (RE-40) was used because its peak power output(500 W) is much larger than the measured peak power in human ankle during walking ( 350 W). Furthermore, it only weighs 0.45 kg and its stall torque and the maximum angular velocity of the motor are up to 2.5 Nm and 7580 rpm, respectively [44].

Using the results in Figs. 4-5, the system required to have a total transmission ratio $R_{total} = 133$ for the given motor and torque-speed constraint. To implement the drive train system, a 3mm pitch linear ballscrew and a timing-belt drive transmission (ratio=1.7:1) between the motor and the ballscrew were used, i.e. $R \sim 3560$. The translational movement of the ballscrew causes an angular rotation of the ankle joint

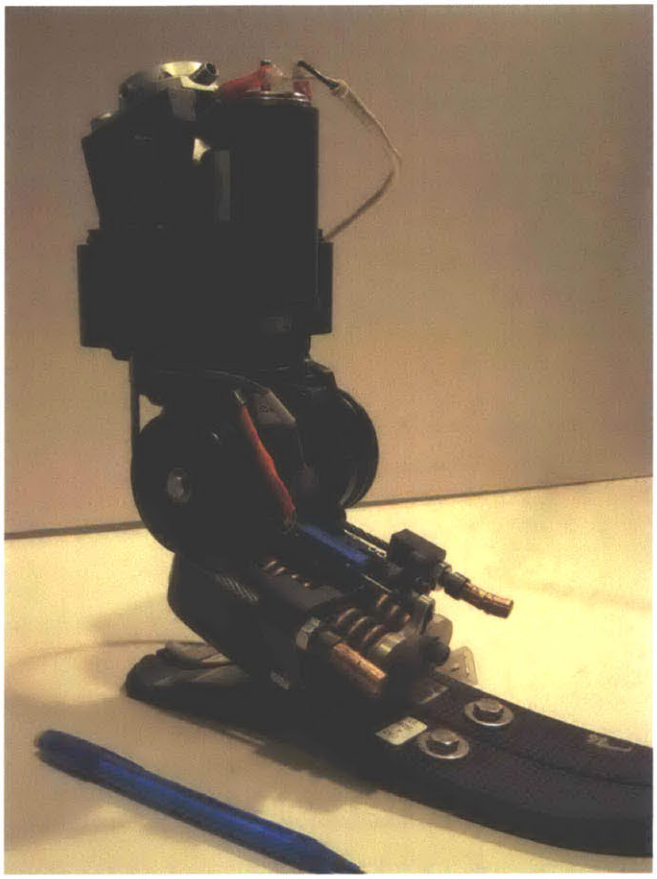

(a) Lateral View

(b) Side View

Figure 4-13: Pictures of the actual prototype.

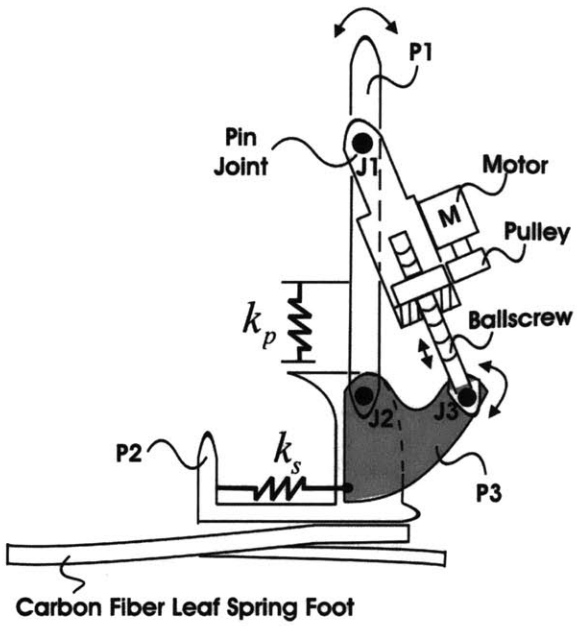


Figure 4-14: Schematics of the actual prototype. Torque is transmitted from motor through timing-belt drive, to the ballnut of the ballscrew. The rotational motion of the ballnut is converted to linear motion of the ballscrew along the line passing through the pins J1 and J3. This linear force is transmitted via rigid link P3 into a compression force on the series springs $k_s$. The other end of the spring pushes on the structure P2 that is attached to joint J2.

via a moment arm $r$=0.0375 m and the series spring (Fig. 4-12(b)). The transmission design of a planetary gearhead with a bevel gear [26] was not adopted to implement the drive train because the peak torque requirement of an intact ankle often exceeds the torque tolerance of the planetary gearhead. Furthermore, using such a transmission combination often makes the height of the prosthesis taller than the existing one.

### Series Spring

According to [42], the selection of the series spring is mainly based on the large force bandwidth criteria. The stiffer the spring is, the higher the SEA bandwidth is at large force. The goal is to choose a series spring such that the large force bandwidth of the SEA is at least two or three times greater than the required force bandwidth.

Based on the results in Fig. 4-10, I selected a series spring with a spring constant $k_s$ equal to 1200 kN/m. With the proposed series and parallel springs, the large force bandwidth of the prosthesis is almost 3 times larger than the required one (Fig. 4-10). Of course, we can always choose a stiffer series spring to further boost up the system performance, however, it will lower the system's ability in shock absorption and stability of the interaction control [42][52]. Furthermore, the stiffer the series spring is used, the more precise measurement of the linear displacement of the series spring is required. This requires for the development of a very high quality analog

electronics to sense the linear displacement of the series spring. Regarding the above tradeoffs of using a stiffer spring, we decided to use the proposed spring constant for the series spring.

The series spring was implemented by 4 compression springs which were preloaded and located on the foot(Fig. 4-5). A detailed descriptions of the ankle mechanism is discussed in [26].

### Parallel Spring

A linear parallel spring $k_p$ with a moment arm $R_p$ in Fig. 4-1 provides a rotational joint stiffness $K_p^r$,

$$K_p^r = (k_p)(R_p)^2 \tag{4.14}$$

The goal is to properly select the moment arm and the spring constant in order to provide the suggested offset stiffness in Table 4.1. In the physical system, due to the size and weight constraints, $k_p$ and $R_p$ were chosen to be 770KN/m and 0.022 m, respectively. Consequently, $K_P^r$=385 rad/s. Because this value is smaller than the suggested offset stiffness(550 rad/s), the SEA supplements the required joint stiffness (see Fig. 4-2). In Fig. 4-10, the simulation result suggests that the current design of the parallel spring is necessary to meet the force bandwidth requirement of the prosthesis.

As shown in Fig. 4-12, the parallel spring was implemented by 4 separate die springs (each with a spring constant equal to 192 Nm/m), two on each side of the structure. There are cables wrapping around a pulley ($R_p$=0.022 m) on each side to stretch the die springs when the joint angle are larger than zero degree.

## 4.5.2 System Characterization

In this section, I present the experimental results of the study of the open-loop characteristics of the physical prototype. The main goals of the experiment are (1) to see to what extent the proposed linear model can predict the actual system behaviors (see Fig. 4-9); and (2) to obtain the actual system parameters including $M_e$ and $B_e$. During the experiment, both ends of the prosthesis were fixed and the parallel spring was disengaged(see Fig. 4-15). The prosthesis was controlled by an onboard computer (PC104) with a data acquisition card and the dc motor of the prosthesis was powered by a motor amplifier. A linear potentiometer was installed across the flexion and extension of the series springs to measure their displacement and was used to estimate the output force. More detailed information for the electronic system of the prosthesis can be obtained in Section 5.4.

Both open-loop step response and the frequency response tests were conducted on the actual system. The result of the open-loop step response is shown in Fig. 4-16. As was illustrated, there was about 8 ms time delay in the system. In addition, the actual step response decayed immediately right after the first overshoot. This discrepancy would seem to stem from the stiction effect of the SEA [42]. The settling time of the open-loop step response was 80 ms.

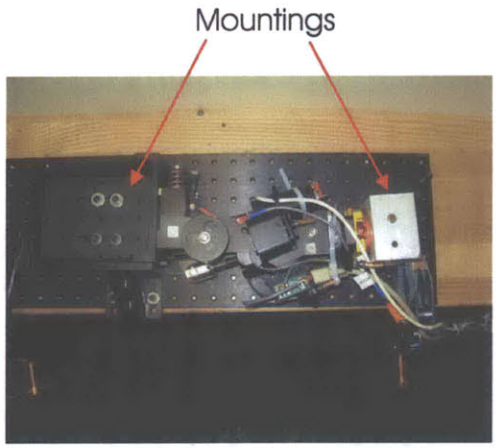


Figure 4-15: Experimental setup for the system characterization.

To measure the frequency response of the system, a chirp signal was applied directly to the motor. The chirp had an amplitude of 4.66 A and varied from 0.01 Hz to 30 Hz in 30 seconds. The force associated with the input current was calculated based on the motor specifications and the transmission ratio. The output force was obtained by measuring the deflection of the series spring (see Fig. 4-17). An open loop Bode plot was plotted for the system based on the input-output from the chirp command (Fig. 4-18).

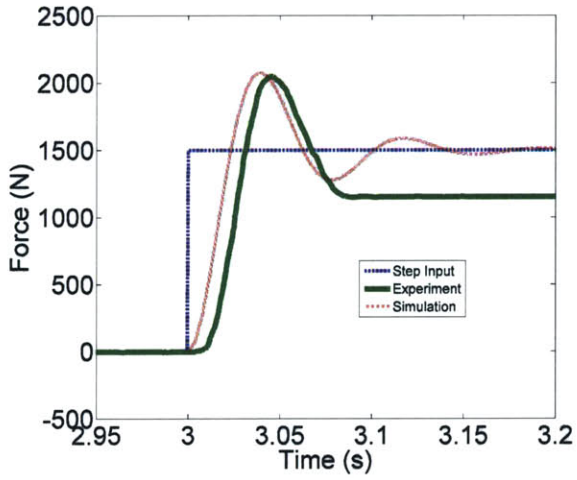


Figure 4-16: Experimental open-loop step response.

In general, the experimental results matched with the simulation of the spring-mass-damper system in Fig. 4-18. The measured resonance frequency of the system at an input force $F_e$= 1000 N (or input torque $T$=37.5 Nm) was about 10.4 Hz. The parameters $M_e$ and $B_e$ were estimated by fitting a second-order model to the measurement data, i.e. $\tilde{M}_e$=250 kg, $\tilde{B}_e$=8250 Ns/m.

It is also observed that the low frequency gain of the open-loop frequency response of the actual system did not remain constant, compared to the simulated one. This

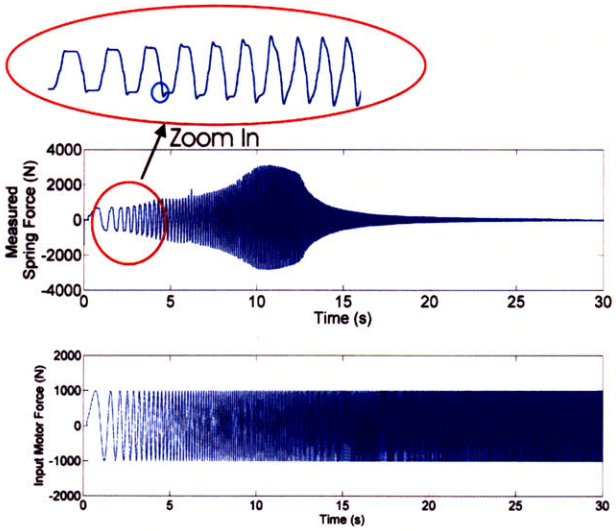


Figure 4-17: Time domain plot for the chirp response. At low frequency, small peaks occurred when the motion was reversed. This discrepancy would seem to stem from the stiction effect of the SEA [42]

discrepancy would seem to stem from the stiction effect of the SEA [42]. Furthermore, the actual frequency response started to roll off earlier than the simulated response. This suggests that there is an extra pole at high frequency in the actual system, which may be due to the combination of the velocity saturation of the motor and motor amplifier saturation.

Fig. 4-19 shows a comparison of experimental open-loop frequency response of the system for different input forces $F_e$. As described in Section 4.4.2, when the output/spring force increased, the system performance decreased due to the motor saturation. The actual open-loop force bandwidth of the prosthesis at $F_e = 1500$ N (56.25 Nm) was 12.6 Hz, which is sufficiently larger than the required force/torque bandwidth (Fig. 4-10).

## 4.6 Discussion

### 4.6.1 Feasibility of the Model

In general, it was shown that the proposed second-order model can capture the dominant dynamic behaviors of the actual system. Incorporating an extra pole at high frequency (>11 Hz) may better describe the actual system with motor amplifier saturation. Given the force bandwidth requirement (3.5 Hz) in this application, the second-order model is still sufficient for our application and can be used for control system design.

Furthermore, as expected, for a small output force and low frequency movement, the actual system behaved nonlinearly due to the stiction and slacking in the transmission. In fact, it is challenging to model such kind of nonlinearity precisely [45].

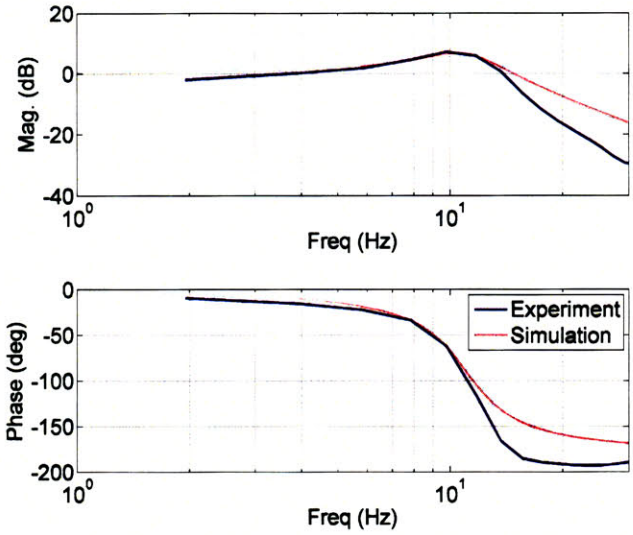


Figure 4-18: Experimental open-loop frequency response at an input force $F_e = 1000N$.

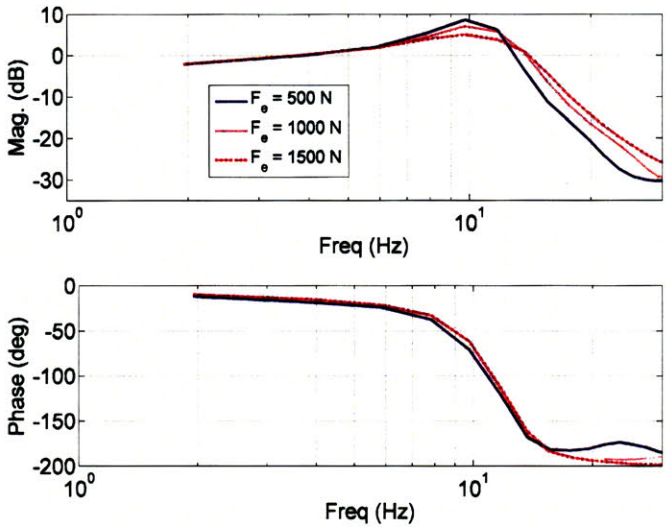


Figure 4-19: A comparison of experimental open-loop frequency response of the system at different input forces $F_e$=[500 N, 1000 N, 1500N].

Definitely, to obtain a precise control over the prosthesis, further study on the topics of stiction and high-order model description for the actual system is required. As the main concern in this thesis is to ensure that the prosthesis can provide a sufficient amount of power to test the hypothesis, the study of the stiction effect is limited for the purpose of improving the peak power output of the system. In the next chapter, I will talk about how to use some control system techniques to partially compensate the stiction in the transmission to augment the system performance.

### 4.6.2 Design Architecture

The prosthetic ankle-foot system requires a high mechanical power output at a large peak torque. In this thesis, I proposed a design structure that uses a parallel spring with a force-controllable actuator with series elasticity. The parallel spring shares the payload with the force-controllable actuator, thus the required peak force from the actuator system is significantly reduced. Consequently, a smaller transmission ratio can be used, and a larger force bandwidth is obtained.

It is always interesting to see if there is any alternative architecture that can satisfy the design requirement. In fact, some researchers [46][47] have suggested to apply the catapult concept for the development of the powered ankle-foot prosthesis/orthosis, through the usage of a series elastic actuator. They have shown that this method can maintain power optimizations to 1/3 of direct drive needs at a weight 8 times less than that for a direct drive solution [47]. However, this method requires a long soft series spring for energy storage which may make the packaging problem harder. Furthermore, a non-backdrivable transmission is required that lowers down the efficiency of system. In the future, it may be useful to compare and analyze the efficiency of these two approaches and it may lead to a more energy efficient design architecture.

Besides, the basic architecture of parallel and series elasticity may also prove useful for other types of assistive devices that require both high power and torque output, such as a hip-actuated orthosis [59].

# Chapter 5

# Control System Design

This chapter presents a control system architecture that allows the prosthesis to mimic the target stance phase behavior. I begin this chapter by describing the overall architecture of the system. Then, I present the development of three basic low-level servo controllers. I further propose a finite state machine that manages the low-level servo controllers to provide the target stance phase behavior during each gait cycle. Finally, I describe the implementation of the controller and present the results of basic gait test to evaluate the performance of the controller.

## 5.1 Overall Control System Architecture

Finite-state control approach are usually used in locomotion assistive/prosthetic devices such as A/K prostheses [9][54]-[57] because gait is repetitive between strides and, within a stride, can be characterized into distinct finite numbers of sub-phases. According to Section 2.1, human ankle also demonstrates such kind of periodic and phasic properties during walking. This motivates the usage of a finite-state controller to control the powered prosthesis.

Referring to Section 3.1, the finite-state controller should be designed to replicate the target stance phase behavior. In order to apply the finite-state control approach to solve this problem, the control system needs to fulfil the following requirements:

- The control system must have three types of low-level servo controllers to support the basic ankle behaviors: (i) a torque controller; (ii) an impedance controller; and (iii) a position controller.

- The finite-state controller must have sufficient numbers of states to replicate the functional behaviors for each sub-phase of human ankle during walking.

- Local sensing is favorable for gait detection and transition among states. The finite-state controller uses these sensing information to manage the state transitions and determine which low-level servo controller should be used to provide proper prosthetic function for a given state condition.

In this project, a control system with a finite-state controller and a set of low-level servos controllers was implemented. The overall architecture of the control system is shown in Fig. 5-1. As can be seen, the control system contained the suggested low-level servo controllers to support the basic human ankle functions. Furthermore, only local sensing variables, including ankle angle, ankle torque, and foot contact were used for state detection and transition. In addition, it also had a finite state machine to manage and determine the transitions among the low-level servo controllers. The finite state machine comprised a state identification and a state control. The former was used to identify the current state of the prosthesis while the latter was used to execute the predefined control procedure for a given state.

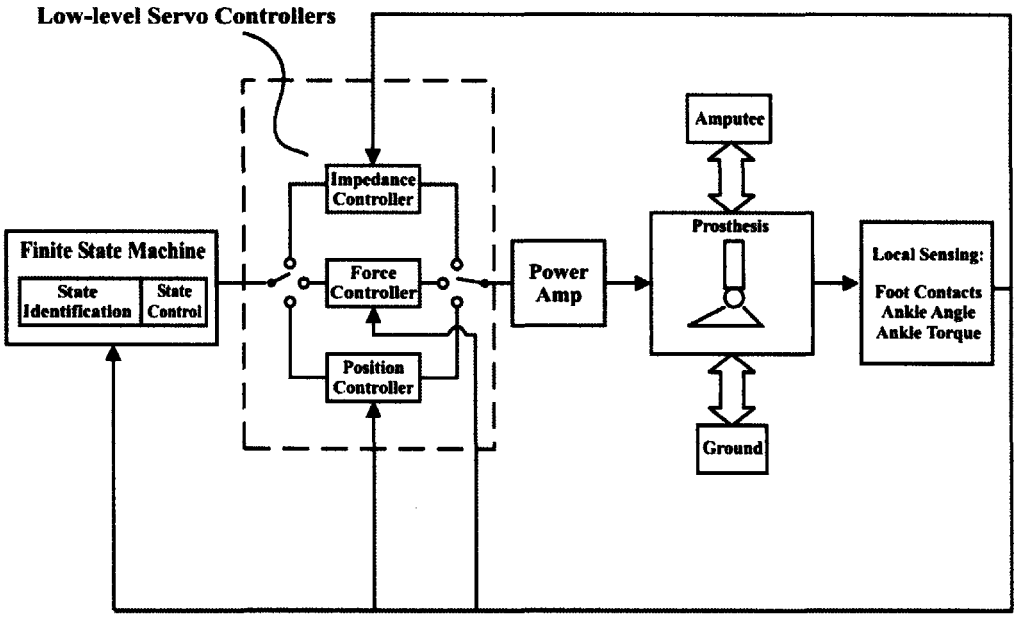


Figure 5-1: Overall control architecture of the prosthesis.

In the following sections, I first discuss the development of the low-level servo controllers, followed by the design of the finite state machine.

## 5.2 Low-level Servo Controllers

As the primary focus of this thesis was not on the advancement of low-level servo controllers, I simply used standard control techniques to design the controllers. Because of this fact, I only briefly discuss the design of the each low-level servo controllers in the following sections.

### 5.2.1 Torque Controller

A torque controller was designed to provide the offset torque and facilitate the stiffness modulation. The primary design concern is to satisfy the bandwidth constrain

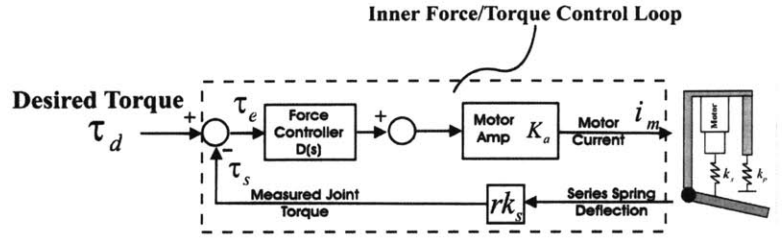


(a) Torque controller

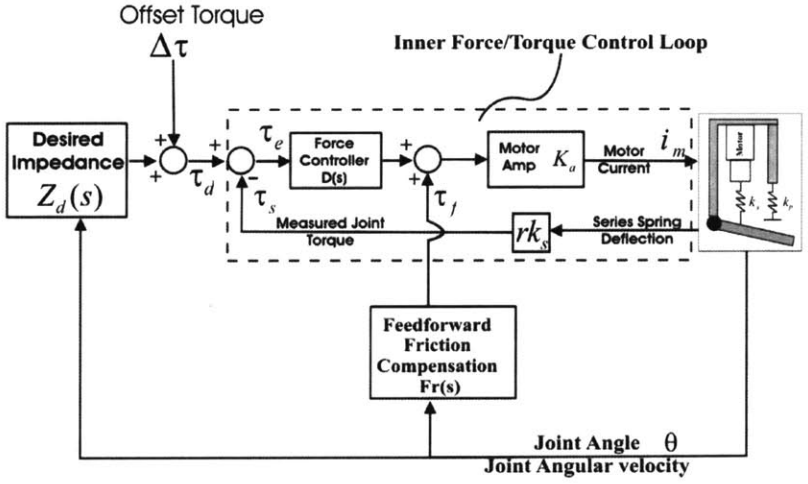


(b) Impedance controller

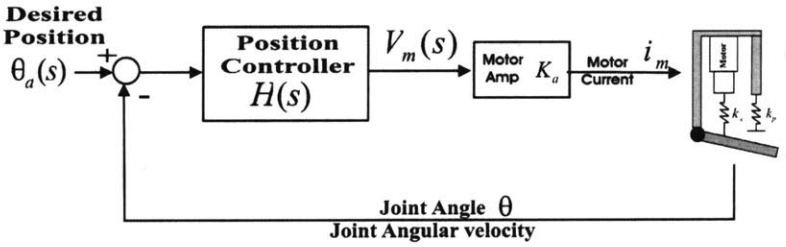


(c) Position controller

Figure 5-2: Block diagrams for the low-level servo controllers.

specified in Table 4.3. A torque controller was proposed, that used the force feedback, estimated from the series spring deflection, to control the output joint torque of the SEA [42] ( Fig. 5-2).

The torque/force controller $D(s)$ was essentially implemented based on a PD control law:

$$D(s) = \frac{V_m(s)}{\tau_e(s)} = K_F + sB_F\frac{p}{s+p} \tag{5.1}$$

where $\tau_e$,$V_m$ are the output torque error and input voltage to the motor amplifier, respectively. Furthermore, $K_F$ and $B_F$ are the proportional gain and damping of the control law, respectively. A simple dominant pole filter $\frac{p}{s+p}$ was incorporated into the controller because often, the measured force signal is very noisy and must be filtered before a derivative may be taken. The pole $p$ of the controller was set to 100 Hz (188.5 rad/s), which is sufficiently larger than the dominant frequency of the human ankle during normal walking. In practice, this filter was also found to be useful to prevent the instability occurred during the transition from a free end condition to a fixed end condition [48]. Using the pure P or PD control, if the prosthesis hit a hard boundary such as the end stop of the prosthesis, it bounced back due to the large impact force seen in the sensor (spring) and eventually exhibited limit cycles. The proposed filter was thought to "filter out the components of the signal which were exciting the unstable dynamics" [48].

The desired motor force (or input voltage $V_m$) was then sent to the motor amplifier to create a force on the motor mass. A current/torque-controlled mode servomotor was adopted in my model Using the current/torque-controlled mode, for a given desired force (or input voltage $V_m$), the motor amplifier outputs a current $i_m$ into the motor according to an amplifier gain $K_a$. The input motor force $F_e(s)$ is equal to $RK_tK_aV_m(s)$, where $K_t$ is the torque constant of the motor. If $K_{total} = RK_tK_a$ that converts voltage into input motor force, i.e. $F_e(s) = K_{total}V_m(s)$.

Using the controller $D(s)$ and open-loop model with the fixed-load condition in Eqn. 4.12, the close-loop transfer function between the actuator force output $F_s$ and the desired output force $F_d$ can be written as:

$$\frac{F_d}{F_s} = \frac{(K_F + B_F s\frac{p}{s+p})K_{total}G_{fixed}(s)}{1 + (K_F + B_F s\frac{p}{s+p})K_{total}G_{fixed}(s))}. \tag{5.2}$$

The controller gains were chosen based on the standard root-locus technique to obtain reasonable force control performance. $K_F$ and $B_F$ were set to be 4 and 20. A simulation of the frequency response of the closed loop system is shown in Figs. 5-3. To convert the actual force into voltage, a gain $K_{fv}$ was multiplied to the controller $D(s)$ in the simulation. All the parameter values for the controller have been listed in Table 5.1.

As indicated in Fig. 5-3, the bandwidth of the closed-loop system (57.6 Hz) was shown to be much larger than the required bandwidth (3.5 Hz). In practice, due to the velocity saturation of the motor and motor amplifier saturation, the actual closed-loop can be significantly less than the expected one.

Table 5.1: Controller Parameters

| Parameters | $K_F$ | $B_F$ | $p$ | $K_a$ |
|---|---|---|---|---|
| Values | 4 | 20 | 100 Hz | 3.6 A/V |
| Parameters | $K_t$ | $K_{total}$ | $K_{fv}$ | $f_c$ |
| Values | 0.0603 Nm/A | 773 N/V | 0.0013 V/N | 0.03 |
| Parameters | $b_c$ | $K_1$ | $K_2$ | |
| Values | 0.31 | 1 | 10 | |

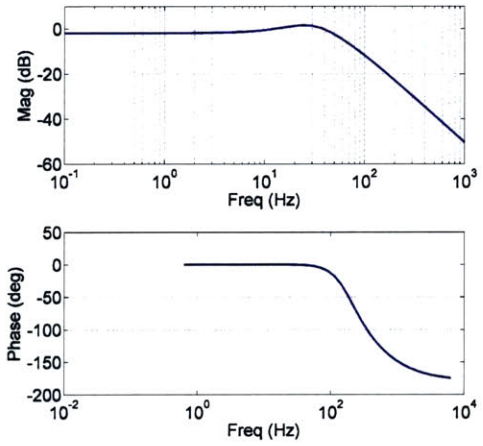


Figure 5-3: Simulation of the closed-loop frequency response.

### 5.2.2 Impedance Controller

An impedance controller was designed to modulate the output impedance of the SEA, especially the joint stiffness. The impedance controller consisted of three main components: (1) Outer position feedback loop, (2) Inner loop force controller, and (3) feedforward friction compensation (Fig. 5-2(b)). The outer loop impedance controller was based on the structure of the "Simple Impedance Control", proposed by Hogan [49][50]. The key idea behind the impedance control is to use the motion feedback from the ankle joint $(\theta, \dot{\theta})$ to increase the output joint impedance. The controller or desired output impedance of the SEA in S-domain is defined as follow:

$$Z_d(s) = \frac{\tau_d(s)}{s\theta(s)} = (B_d + \frac{K_d}{s}) \tag{5.3}$$

where $\tau_d$, $K_d$, $B_d$ are the desired SEA output joint torque, stiffness, and damping, respectively. Taking into the consideration of the parallel elasticity, the total joint impedance is

$$Z_{total} = \begin{cases} (\mathrm{B}_d + \frac{K_d}{s}) & \theta \leq 0 \\ (\mathrm{B}_d + \frac{K_d + K_p^T}{s}) & \theta > 0 \end{cases} \tag{5.4}$$

Due to the intrinsic impedance (e.g. friction and inertia), the actual output impedance consists of desired output impedance due to the controller plus that due

to the mechanism. For this reason, the aforementioned torque controller was incorporated into the impedance controller to reduce the effect of the intrinsic impedance. Although increasing the gain $K_F$ can shadow the intrinsic impedance (e.g. friction or inertia) in the mechanism, it may trigger instability when the system couples to certain environments at high gain [48][53]. One way to augment the torque controller without violating the stability criteria is to use a model-based friction compensation term $F_r(s)$. A standard feedforward friction compensation term was applied into the torque controller and defined as:

$$\tau_f = f_c(\tau)sgn(\dot{\theta}) + b_c\dot{\theta}, \tag{5.5}$$

where $f_c$,$b_c$ are the Coulombic force constant and damping coefficient, respectively [45]. All these parameters were identified using experimental data.

### 5.2.3 Position Controller

A standard PD-controller $H(s)$ was proposed to control the equilibrium position $\theta_1$ of the foot during swing. Then, the input voltage $V_m(s)$ to the motor amplifier is $V_m(s) = K_1(\theta_1 - \theta) + K_2\dot{\theta}$, where $K_1$ and $K_2$ are the proportional and derivative terms of the controllers.

## 5.3 Finite-State Controller

A finite-state controller for level-ground walking was implemented to replicate the target ankle behavior (Fig. 5-4). The controller comprises of two parts: stance phase control and swing phase control. Each part of the controller contains three states and the details are discussed as follows.

### 5.3.1 Stance Phase Control

Three states (CP, CD, and PP) were designed for stance phase control. The stance phase control for a typical gait cycle is graphically depicted in Fig 5-4. Detailed descriptions for each state are shown below.

- CP begins at heel-strike and ends at mid-stance. During CP, the prosthesis outputs a joint stiffness[1], $K_{CP}$ to prevent foot slapping and provide shock absorption during heel-strike.

- CD begins at mid-stance and ends right before PP or toe-off, depending on the measured total ankle torque $T_{ankle}$. During CD, the prosthesis outputs a joint stiffness, $K_{CD}$ to allow a smooth rotation of the body, where $K_{CD} = K_p^r + K_{CD1}$.

[1]The conversion of the joint stiffness between translational and rotary domains is $K = r^2k$, where $k$ and $r$ are the joint stiffness in translational domain and moment arm, respectively. For example, $K_{CP} = r^2k_{CP}$.

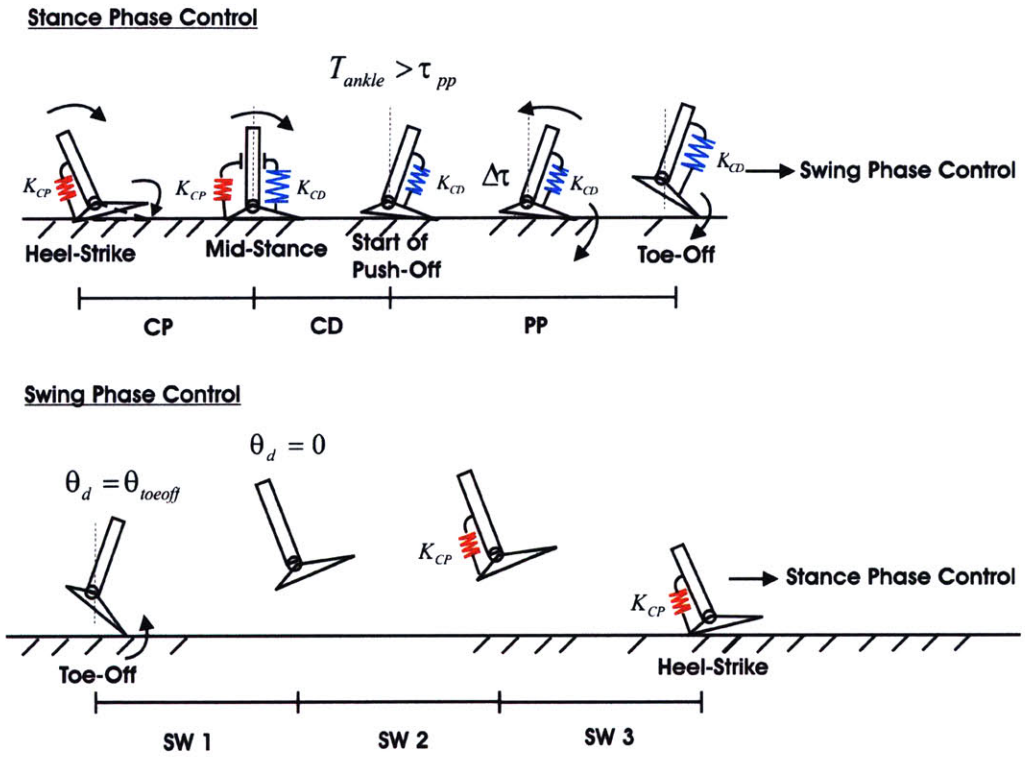


Figure 5-4: The finite-state control for a typical gait cycle.

- PP begins only if the measured total ankle torque, $T_{ankle}$ is larger than the predefined torque threshold, $\tau_{pp}$, i.e. $T_{ankle} > \tau_{pp}$. Otherwise, it remains in state CD until the foot is off the ground. During PP, the prosthesis outputs a constant offset torque, $\Delta\tau$ superimposing the joint stiffness, $K_{CD}$ as an active push-off.

$K_{CP}$, $K_{CD}$, $\tau_{pp}$, and $\Delta\tau$ are the main parameters affecting the ankle performance during the stance phase control. In particular, the offset torque is directly related to the amount of net work done at the ankle joint. These parameter values were chosen based on the user's walking preference during experiments.

### 5.3.2 Swing Phase Control

Another three states (SW1, SW2, and SW3) were designed for the swing phase control(see Fig 5-4). Descriptions for each state are shown below.

- SW1 begins at toe-off and ends in a given time period, $t_H$. During SW1, the prosthesis servos the foot to a predefined foot position, $\theta_{toeoff}$ for foot clearance.
- SW2 begins right after SW1 and finishes when the foot reaches zero degree. During SW2, the prosthesis servos the foot back to the default equilibrium position $\theta_d = 0$ to prepare for the next heel-strike.

- SW3 begins right after SW2 and ends at the next heel-strike. During SW3, the controller resets the system to impedance control mode and output a joint stiffness, $K_{CP}$.

It is important to have state SW3 in the swing phase control to ensure the control system operating in impedance mode before heels-strike. Because the heel-strike event happens very quickly, there is not enough time for the control system to switch from position control mode to impedance control mode during heel-strike. The time period, $t_H$ and predefined foot position, $\theta_{toeoff}$ were all tuned experimentally.

### 5.3.3 Sensing for State Transitions

During state transition and identification, the system mainly relied on four variables:

- Heel contact(H). H=1 indicates that the heel is on the ground, and vice versa.
- Toe contact(T). T=1 indicates that the toe is on the ground, and vice versa.
- Ankle angle ($\theta$)
- Total ankle torque ($T_{ankle}$)

All these triggering information can be obtained using local sensing; including foot switches to measure heel/toe contact, ankle joint encoder to measure the ankle angle, and the linear spring potentiometer to measure joint torque. The hardware implementation of these local sensing will be discussed in the next section. The finite-state control diagram indicating all triggering conditions is shown in Fig. 5-5.

## 5.4 Controller Implementation

In this section, I describe the electronics hardware used for implementing the proposed controller onto the MIT powered ankle-foot prosthesis, including sensing and computing platform. This system platform provides a test bed for testing a broad range of human ankle behaviors and control systems experimentally.

### 5.4.1 Computer System Overview

Fig. 5-6 shows the schematics of the overall computer system. The computer system contained an onboard computer (PC104) with a data acquisition card, power supply, and motor amplifiers. The system was powered by a 48V, 4000mAh Li-Polymer battery pack. Custom signal conditioning boards amplified sensor (linear pot) reading and provided a differential input to the data acquisition board, in order to minimize common mode noise from pick-up in the system. A custom breakout board interfaced the sensors to the D/A board on the PC104 as well as provided power to the signal conditioning boards.

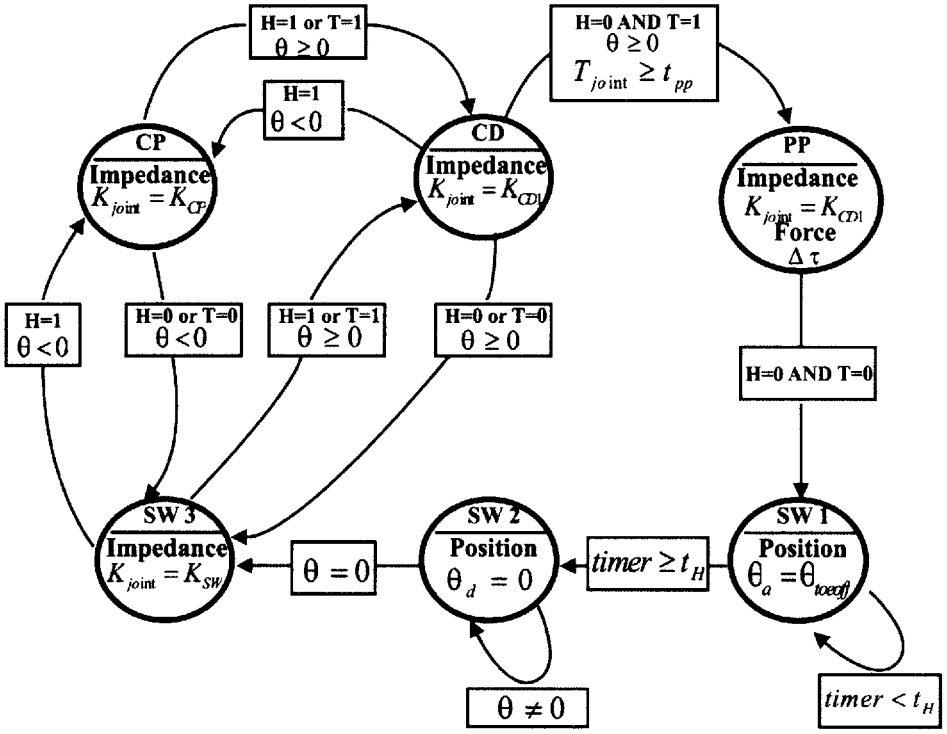


Figure 5-5: The finite-state controller for level-ground walking.

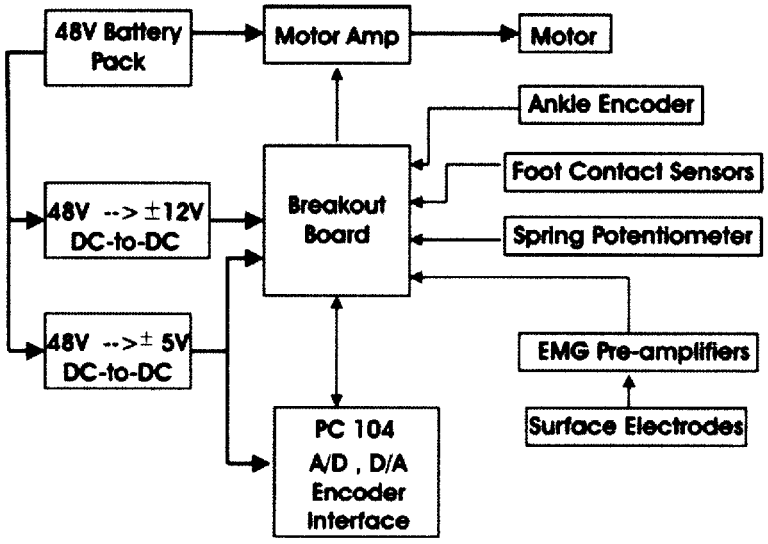


Figure 5-6: Schematics of the overall computer system.

### 5.4.2 PC104 and Data Acquisition

The PC used was a MSMP3XEG PC/104 from Advanced Digital Logic, Inc. It was a miniature modular device that incorporated most of the major elements of a PC compatible computer in a small form factor. It was fitted with a PENTIUM III 700 MHz processor.

A PC/104 format multifunctional I/O board (Model 526) from Sensory Co. was connected to the PC/104. It had 8 differential analog inputs, 2 analog outputs, and 4 quadrature encoder counters. Matlab xPC Target was used to run the algorithm for real-time control and data acquisition. The Matlab xPC real-time kernel was installed and run on the PC/104 (remote PC). A model was created using Simulink Matlab xPC Target, which allowed I/O blocks to be added to the model. The model was compiled on the host PC using Matlab Real-Time Workshop and a C++ compiler created executable code. The executable code was downloaded from the host PC to the target PC via TCP/IP and the code was run on the target in real-time. Data were recorded by using the xPC host scopes in the Simulink model. During the program running, the target PC (PC104) could communicate with the host computer via Ethernet. The host computer could send control commands and obtain sensory data from the target PC104. The dc motor of the prosthesis was powered by a motor amplifier (Accelnet Panel ACP-090-36, V= 48volts, Ipk = 36A) from Copley Controls Corp.

### 5.4.3 Sensors

Three state variables, including heel/toe contact, ankle angle, and joint torque, were measured to implement the proposed finite-state controller. I installed a 5 k$\Omega$ linear potentiometer across the flexion and extension the series springs to measure their displacement. I also mounted a 500-line quadrature encoder (US digital, inc.) in between the parent link mounting plate and child link mounting plate to measure the joint angle of the prosthetic ankle. Six capacitive force transducers were placed on the bottom of the foot: two sensors beneath the heel and four beneath the forefoot region. Fig. 5-7 describes the sensors on the powered prosthesis.

### 5.4.4 Mobile Computing Platform

In collaboration with Ernesto Martinez-Villalpando, I developed a mobile computing platform that allowed us to conduct untethered walking experiments outside the laboratory. As shown in Fig. 5-8, the mobile platform was mounted on an external frame backpack. Most of the electronic components were mounted on the platform, including a PC104, a power supply, I/O Cards, and a motor amplifier. Using cabling, the prosthesis was connected to the I/O board and motor amplifier on the platform.

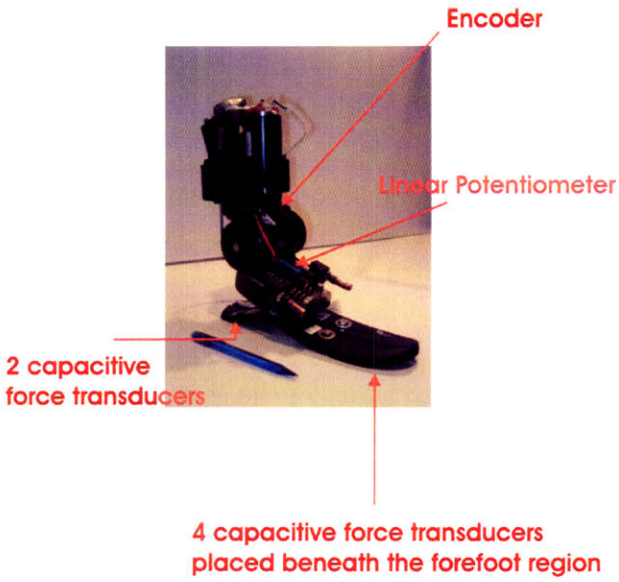


Figure 5-7: Sensors on the MIT powered ankle-foot prosthesis.

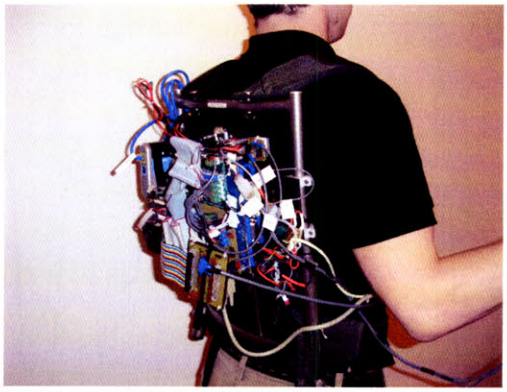

(a) Lateral View

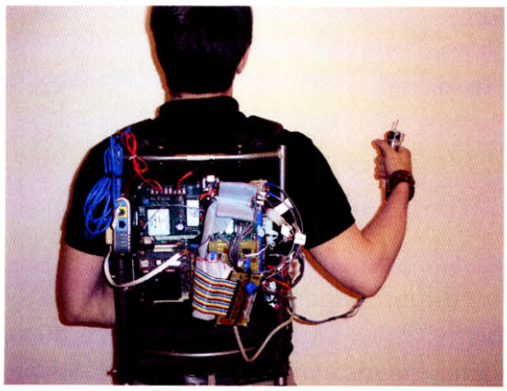

(b) Posterior View

Figure 5-8: A mobile computing platform was designed to provide the capability of testing the system outside the laboratory.

## 5.5 Control System Evaluation

### 5.5.1 Bench Test

I conducted both step response and frequency response tests on the physical prototype to understand the closed-loop performance (with fixed end condition) of the torque/force controller described in Section 5.2.1. The same bench test setup was used as described in Fig. 4-15, in which both ends of the prosthesis were fixed on the ground rigidly.

The proportional and derivative gains of the controller were tuned experimentally by examining the step response of the actuator. Figs. 5-9 shows the controller response to track a step force of 1500 N and a sine wave in force of 1000N at 5 Hz. The corresponding parameters used in the actual were listed in Table 5.1. The simulation can fairly predict the step response of the actual system. To prevent instability occurring during the contact with different environments, the controller gain $K_F$ was set to a relative small value, consequently, the steady state error of the closed-loop control (about 25%) is quite large (see Fig. 5-9(a)). One resolution to this problem was to adjust the desired force by a factor of the steady state error. It has been applied in the experiment of tracking the sine wave in force.

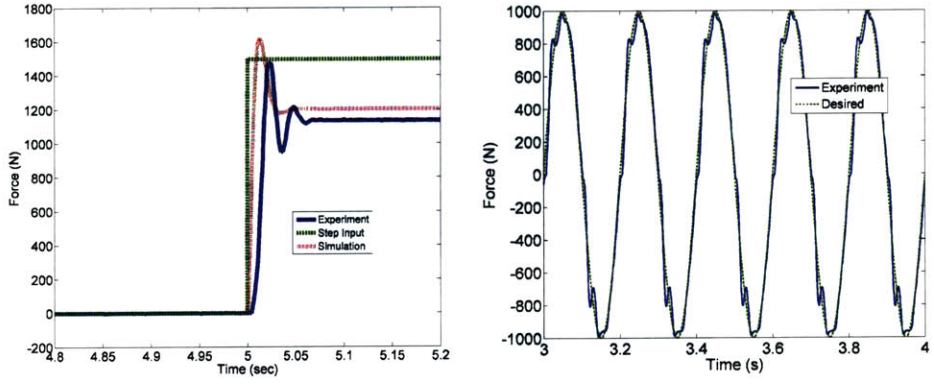


(a) Step Response

(b) Sine Response

Figure 5-9: Tracking performance of the closed-loop force controller in fixed end condition.

To determine the closed-loop bandwidth of the control system, a sine wave chirp in force (500 N) was applied from 0.01 Hz to 40 Hz in 40 seconds. Fig. 5-10 shows both the experimental and theoretical closed loop Bode plots. The measured and theoretical resonance peak were at 21.4 Hz and 51.3 Hz, respectively. Due to the amplifier saturation, the measured frequency response started to roll off much earlier than the simulated one. However, this controller is still sufficient for our application because the required force bandwidth is only 3.5 Hz.

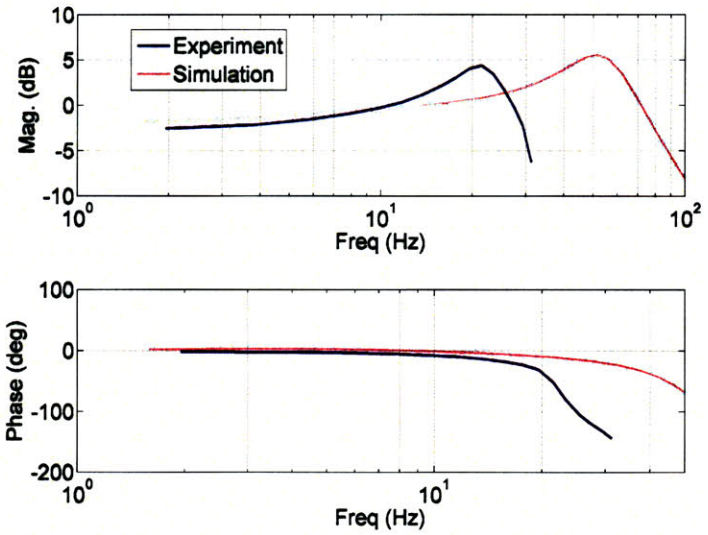


Figure 5-10: Experimental closed-loop frequency response with a desired input force $F_d = 500$ N.

### 5.5.2 Initial Gait Test

Before testing three unilateral amputee participants, I have conducted a substantial amount of basic gait tests with the device on a healthy, bilateral below-knee amputee to evaluate the performance, stability, and robustness of the controller. The amputee wore the powered prosthesis on his right leg and a conventional passive below-knee prosthesis (Ceterus, from Ossur, Inc.) on the left leg. During the experiment, the amputee participant was requested to walk along a 6 foot-long walkway at a self-selected speed. He communicated desired controller parameters such as stiffness values to a separate operator during the walking trials. The results of the basic gait study proved that the proposed finite state machine performed robustly and was capable of mimicking the target stance phase behavior. In the next sections, I present the results of the gait tests for two kinds of system responses (Virtual Spring Response and Active Mechanical Power) to illustrate the actual performance of the control system.

#### Virtual Spring Response

Fig. 5-11 shows real time data for one gait cycle of a walking experiment in which the powered prosthesis was controlled to output a virtual spring response. As was proposed in Fig. 5-5, the system went through the state sequence 1-2-0 for each gait cycle under the virtual spring condition (see Fig. 5-11d). The corresponding ankle torque-angle behavior is shown in Fig. 5-12. This experimental result demonstrates the system's capacity to track the desired stiffness during CP and CD. As can be seen, the actual stiffness curve is slightly off from the desired curve by approximately 3Nm because, in the physical system, the engagement position of the unidirectional parallel spring was not exactly equal to zero degree, or the equilibrium position. This

error caused the motor system to pre-load the spring at the equilibrium position.

It was expected that the measured stiffness curve would show fluctuations during heel strike because the control system was not designed to satisfy such demanding bandwidth requirements during heel-strike. This justifies the use of a SEA as the force-controllable actuator because with series elasticity, even if the movement of the prosthesis is much faster than the bandwidth of the control system, the prosthesis can still behave as a spring to prevent any impact shock to the transmission [42]. Furthermore, there is a heel spring in the compliant foot (Flex-foot) of the proposed prosthesis to reduce additional impact. The subject participant never complained about the performance of the ankle during heel-strike.

### Active Mechanical Power

Fig. 5-13 shows real time data for one gait cycle of a walking experiment in which the powered prosthesis was controlled to deliver positive net work during stance. The system went through a longer state sequence 1-2-3-4-5-0 than that under the virtual spring condition (Fig. 5-13d). It is noted that a dramatic change in joint velocity occurred during SW1 (Fig. 5-13a) due to the controller transition from the impedance controller to position controller during SW1. Furthermore, it is also observed that the power output of the prosthesis during PP behaved differently, as compared to that of normal human ankle [12].

The corresponding ankle torque-angle behavior is shown in Fig. 5-14. The experimental result demonstrates the system's capacity to track the desired target stance phase behavior. As was designed, a constant offset torque $\Delta\tau$ was applied to the amputee participant when the ankle torque was larger than the triggering threshold $t_{pp}$. In this example, $\Delta\tau$ and $t_{pp}$ were set at 50 Nm and 105 Nm respectively, based on the amputee participant's preference. It is noted that the measured ankle torque-angle curve flattens around the peak torque region because the actual system required time (about 50 ms) to output the offset torque during the transition from CD to PP.

Also, the toe-off was set to be triggered before the ankle joint reaches the zero torque level (Fig. 5-14) because it can provide enough time for the control system to switch from impedance control mode to position control mode at the transition from stance to swing. Fig. 5-15 shows a summary of gait test results to demonstrate the prosthesis's capability of doing different amount of work at the joint in a gait cycle.

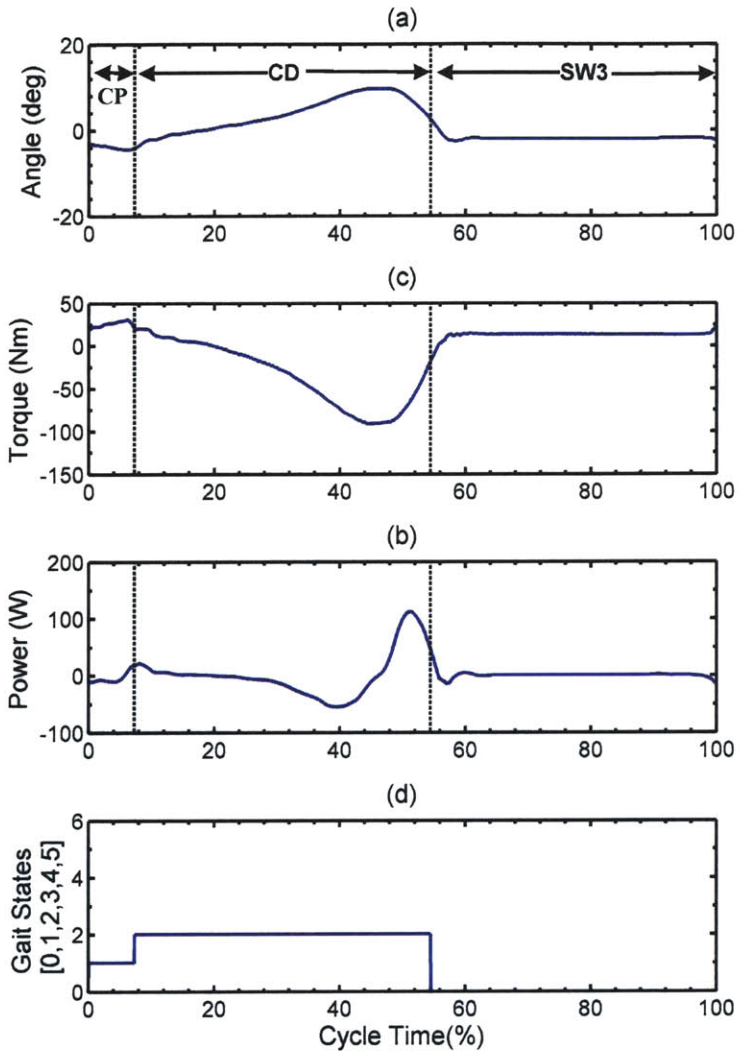


Figure 5-11: Measured ankle angle, torque, power, and the gait states of a walking trial in which the prosthesis behaved as a virtual spring. The gait states are defined as following: CP=1, CD=2, PP=3, SW1=4, SW2=5, and SW3=0. Under the virtual spring control, the system only went through the state sequence 1-2-0 for each gait cycle.

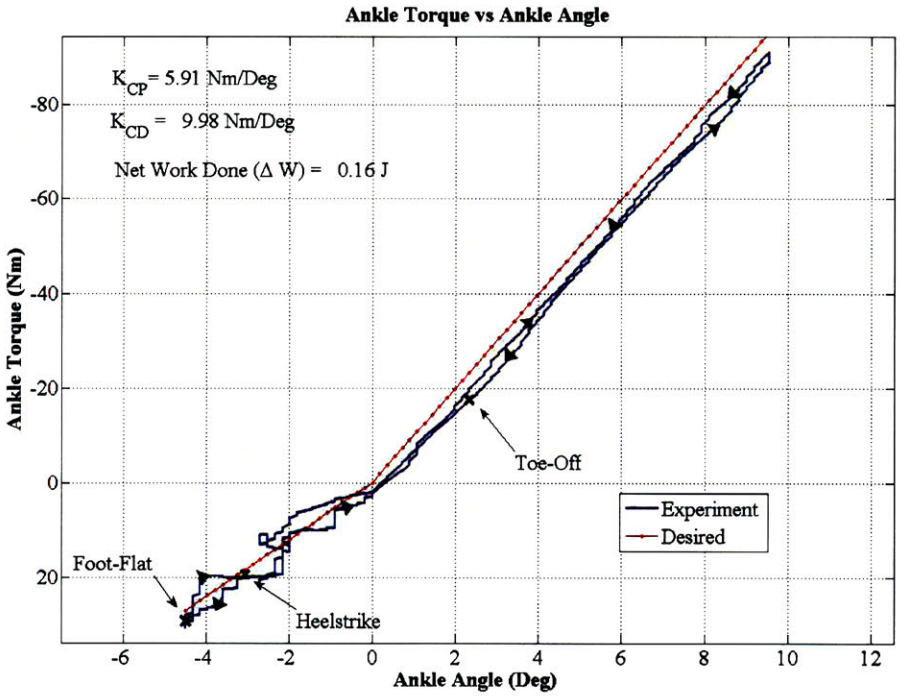


Figure 5-12: An experimental ankle torque-angle plot for the powered prosthesis across a gait cycle using the virtual spring controller.

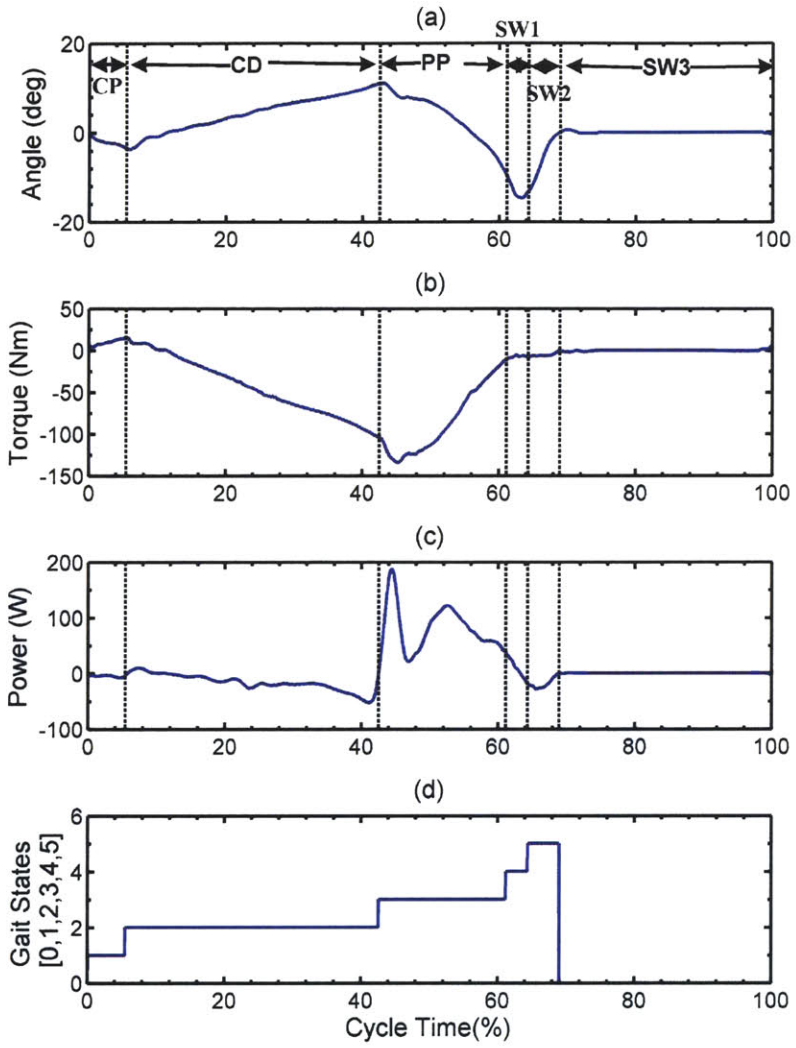


Figure 5-13: Measured ankle angle, torque, power, and the gait states of a walking trial in which the prosthesis performed positive net work. The gait states are defined as following: CP=1, CD=2, PP=3, SW1=4, SW2=5, and SW3=0.

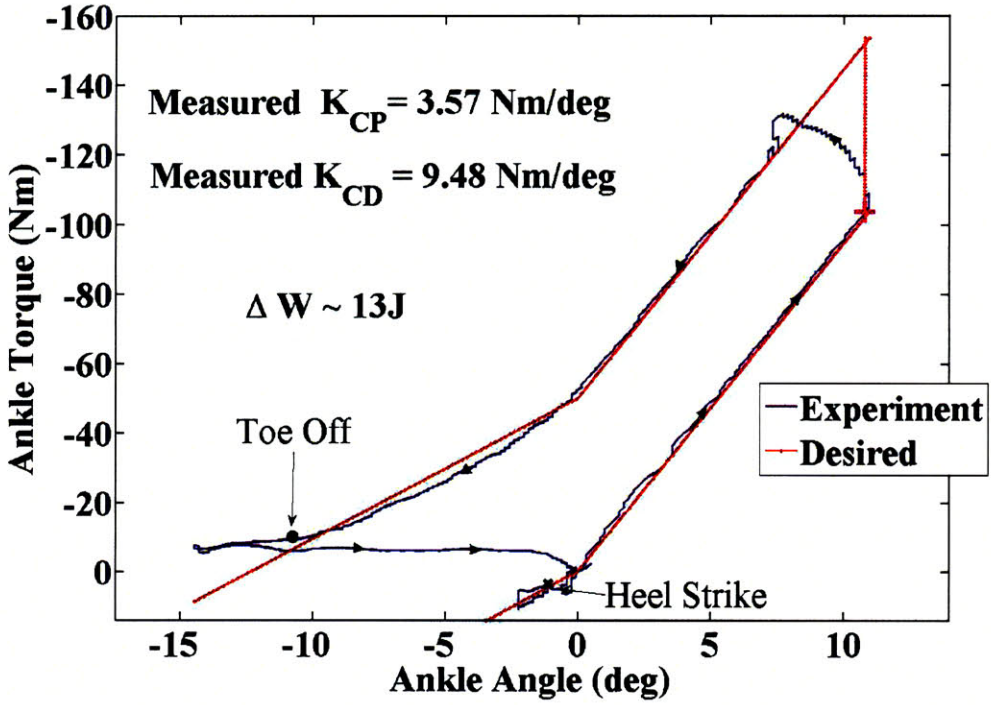


Figure 5-14: An experimental ankle torque-angle plot for the powered prosthesis across a gait cycle with positive net work. The pink cross indicates the time at which the prosthesis begins actively plantar flexing.

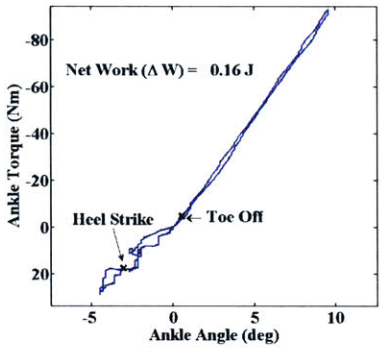


(a) Net Work = 0J

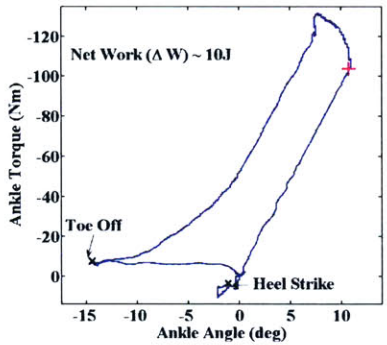


(b) Net Work = 10J

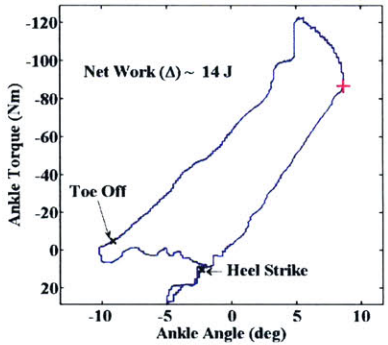


(c) Net Work = 14J

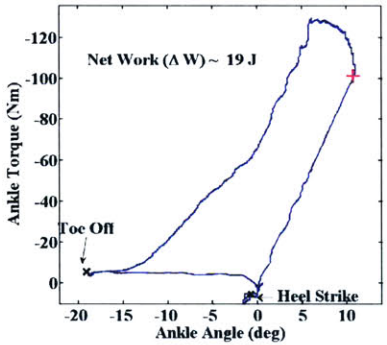


(d) Net Work = 19J

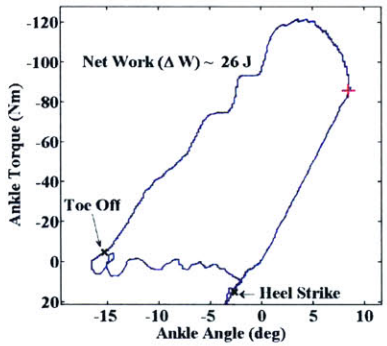


(e) Net Work = 26J

Figure 5-15: Examples of demonstrating the prosthesis's capability of doing different amount of work in a gait cycle.

## 5.6 Discussions

The method of using a constant offset torque was an initial attempt to mimic the active push-off of normal human walking. It was not intent to capture all the nonlinear characteristics of the observed quasi-static stiffness curve, however, it can provide a more intuitive way to relate the user's feedback to the parameter adjustments in the control system during experiments. Because of this fact, it speeds up the process to conduct clinical study for the evaluation of the hypothesis.

In the future development, the control system should be able to provide the active push-off in a way as observed in human walking and also adapt to the user's walking speed. One way to achieve this could be to implement local reflex control as in the muscle reflex by using the positive force feedback. Geyer and coworkers showed that positive force feedback of the extensor muscles leads to self-adaptive joint behavior that not only generates the active push-off in a smooth manner, but also stabilizes the net energy input around a steady-state input [60].

Besides, it is also important to develop a multi-functional control system to deal with the control problems for different locomotion events such as stair descent or ascent. Researchers have shown the feasibility and effectiveness of using the finite-state control approach to solve the control problems of above-knee prostheses for different locomotion events [9][54][55]. I am in the process of extending the current finite state machine for the control of the prosthesis for stair descent and ascent. More detailed will be published soon

# Chapter 6

# Clinical Evaluation

According to the literature [3][4][24], the most effective way to evaluate the performance of a leg prosthesis is to measure the rate of oxygen consumption of an amputee participant walking with the prosthesis. This can lead us to understand and compare the walking economy of an amputee associated with different prostheses.

In this investigation, I study the rate of oxygen consumption of three unilateral transtibial amputees walking at self-selected speeds for three different conditions: (1) using their conventional passive prostheses; (2) using the powered prosthesis with only a virtual spring response; and (3) using the powered prosthesis with a nonconservative, motive power output. Furthermore, to understand gait biomechanics associated with the powered prosthesis and their conventional passive prostheses, I also study the kinematics and kinetics of one of the amputee participants for the experimental conditions (1) and (3).

This chapter describes the methodology and results of the clinical evaluation. I first describe the amputee participants and the experimental protocol. Then, I present the performance metrics using in both the metabolic cost study and gait biomechanics study. Finally, I describe and discuss the results obtained from the clinical study.

## 6.1 Experimental Participants

Three unilateral, transtibial amputees participated in the study. Amputee participants were experienced at prosthesis ambulation, could ambulate at least at a K3 level (i.e. the patient has the ability or potential for ambulation with variable cadence) and had no other musculoskeletal problems or any known cardiovascular, pulmonary or neurological disorders. The three participants (all male) were 40-57 yrs old, 173-176 cm in height, and weighed 71-86 kg. Patient characteristics are summarized in Table. 6.1.

Table 6.1: Amputee participant characteristics and self-selected walking speed

| Subject # | Gender | Age (yrs) | Height (cm) | Weight (kg) | Speed (m/s) | Usual Prosthesis | Cause of Amputation |
|---|---|---|---|---|---|---|---|
| 1 | M | 45 | 176 | 86 | 1.38 | Flex Foot | Trauma |
| 2 | M | 57 | 174 | 71 | 1.45 | Flex Foot | Trauma |
| 3 | M | 40 | 173 | 75 | 1.68 | Freedom | Trauma |

## 6.2 Use of Human Subject Approval

The experiments were approved by MIT's Committee on the Use of Humans as Experimental Subjects (COUHES). The participants were volunteers and were permitted to withdraw from the study at any time for any reason. Before taking part in the study, each participant read and signed a statement acknowledging informed consent. Appendix A includes a copy of subject consent for the COUHES.

## 6.3 Experimental Protocol

The study was divided into three sessions: (I) Basic Clinical Gait Study , (II) Metabolic Cost Study, and (III) Kinematics and Kinetics Study. The first session was performed in the Biomechatronics Laboratory within the Media Lab at MIT. Before testing, each participant was fitted with the powered prosthesis by a professional prosthetist. During the session, each participant was asked to walk along a 30-foot long walkway at a self-selected speed. Each participant communicated desired parameter values to a separate operator during the walking trials. Sensory data (e.g. joint torque and angle) from the prosthesis was captured during the experiment. By the end of the first experimental session, a set of control system parameters was obtained that provided the most favorable prosthetic ankle response at a self-selected walking speed.

In the second session, oxygen consumption data was collected as an indicator of metabolic cost. The experiment were performed at Massachusetts Institute of Technology (MIT) on the Johnson Indoor Track. Before the second session began, each participant had approximately two hours of acclimatization on the powered prosthesis. The rate of oxygen consumption was measured for three conditions: (1) using the participant's conventional passive-elastic prosthesis; (2) using the powered prosthesis with only a virtual spring response; and (3) using the powered prosthesis with a nonconservative, motive power output. Before each trial, a participant was given ten minutes to walk with each prosthesis to acclimatize to the new hardware. Walking speed was controlled by having the participant follow a modified golf caddy set to a desired speed. The self-selected walking speed with the powered prosthesis (condition 3) was used for all three conditions. During the test for conditions (2) and (3), each participant wore the mobile computing platform, including the battery (about 4 kg) to support the control of the powered prosthesis. For condition (1), each participant wore the mobile platform without the battery during the test. As with the first experimental session, sensory data (e.g. joint torque and angle) from the prosthesis was captured during the experiment. Each participant was advised not to have intense or prolonged exercise for 24 hours prior to the experimental session. Furthermore, each participant was instructed to stay hydrated and not to have caffeine or a heavy meal three hours before the experimental session.

The third session was performed in the MIT Motion Analysis Laboratory in CSAIL to study differences in kinematics and kinetics associated with the experimental conditions (1) and (3). This analysis may provide us biomechanical mechanisms for the

results obtained in the second session. Each participant was asked to walk at a self-selected speed along the walkway for the experimental conditions (1) and (3). As with the second session, during the test for condition (3), each participant wore the mobile computing platform, including the battery (about 4 kg), while for condition (1), each participant wore the mobile platform without the battery during the test. Each amputee participant was given time to acclimatize to each condition before testing. Both kinematic and kinetic data were measured during each walking trial and compared with respect to the unaffected and affected sides of each unilateral amputee participant.

## 6.4 Performance Index - Metabolic Cost of Transport

The metabolic cost of transport (COT) has been widely used to evaluate the performance of prosthetic leg interventions [3][4]. The COT is a dimentionless number defined as the metabolic energy required to transport unit body weight unit distance, or

$$C_m = \frac{MetabolicEnergy}{TotalWeight * DistanceTraveled} \tag{6.1}$$

where $C_m$ is the metabolic COT. The total weight in Eqn. (6.1) is the weight of the participant plus the prosthetic system. The distance traveled was obtained by multiplying the walking speed by the time period $T$ for which the total energy was calculated.

The net metabolic energy $E_m$ is normally obtained by integrating the net metabolic energy expenditure rate $\dot{E}_m$ for a given time period $T$.

$$E_m = \int_0^T \dot{E}_m dt \tag{6.2}$$

Equation (6.1) becomes

$$C_m = \frac{E_m}{Mg\nu T}, \tag{6.3}$$

where $M$, $g$, and $\nu$ are the mass of the participant plus the prosthetic system, gravity constant, and the average forward speed, respectively. The resultant metabolic rate was obtained by subtracting the resting metabolic rate from the metabolic cost of walking.

## 6.5 Measurement of Metabolic Cost of Transport

The energy cost was estimated from $O_2$ consumption and $CO_2$ production measured with a portable K4 telemetric system [61]. The K4 system includes a portable unit worn by the participant and a base station where the data are recorded. The portable unit weighs 1.5kg and consists of a silicon mask containing a flow-rate turbine which

was fixed to the subject's face. A processing unit containing the $O_2$ and $CO_2$ analyzers was placed on the participant's chest and a transmitter/battery pack was placed in the backpack.

During each walking trial, the participant walked on the track for 5 minutes while metabolic data was recorded. Rest measurements were taken while the participant was seated for 5 minutes before and after each walking trial and the average resting value was calculated. The resting $\dot{V}_{O_2}$ and $\dot{V}_{CO_2}$ values were subtracted from the walking trial data to give the net values of $\dot{V}_{O_2}$ and $\dot{V}_{CO_2}$(ml/s). These values were then used to estimate the net metabolic rate $\dot{E}_m$ for each walking trial using the formula from [62]:

$$\dot{E}_m = 16.48\dot{V}_{O_2} + 4.48\dot{V}_{CO_2} \tag{6.4}$$

The total cumulative energy for the walking trail was then plotted using the Eqn. (6.2). When the data showed a line of constant slope, steady state energy consumption occurred. I used the steady state portion of the net metabolic energy to compute the metabolic cost of transport for each walking trail.

## 6.6 Data Processing and Analysis of the Kinematics and Kinetics Study

The kinematic and kinetic data were measured using a motion analysis system (Vicon 512 system;Oxford Metrics, UK). Kinematics were derived by measuring the three-dimensional positions of reflective markers which were placed in different locations on each amputee participant during the test. Kinematics were computed from measures of ground reaction forces (GRFs) derived using two staggered force platforms(AMTI Inc.,MA) embedded in the walkway. The center of mass (COM) kinematics (linear acceleration, velocity, and position) were calculated from three-dimensional GRF data [63][64].

In the gait analysis, I evaluated the walking biomechanics of each amputee participant based on the following metrics:

1. gait symmetry between the unaffected and affected sides
2. vertical GRFs for both leading and trailing legs.
3. external work done on the COM by each limb

The detailed descriptions and explanations for each metric are shown below.

### 6.6.1 Gait Symmetry

One way to compare the gait patterns for different experimental conditions is to look at the gait symmetry between the affected and unaffected sides [8][7][65]. It is assumed that normal gait is symmetrical and that deviation from a reference pattern is a sign of disability [24]. To analyze the spatial asymmetry, I compute the root-mean-square

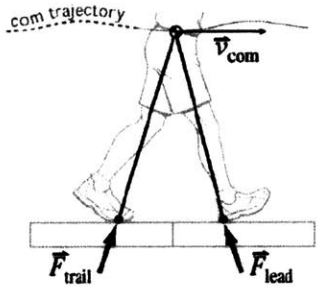


Figure 6-1: A simple model of bipedal walking [64]. This model shows the velocity of the center of mass, $\vec{v}_{cm}$, and ground reaction forces acting on trailing, $\vec{F}_{trail}$, and leading, $\vec{F}_{lead}$, legs during double support phase.

(RMS) error between the kinematics (hip, knee, and ankle angles) of the unaffected and affected sides for a gait cycle:

$$RMS = \sqrt{\frac{1}{N}\sum(\beta(i)_{unaffected} - \beta(i)_{affected})^2} \tag{6.5}$$

, where $\beta(i)_{affected}$ and$\beta(i)_{unaffected}$ are the joint angles (hip or knee or ankle) at $i$ time instant for the affected and unaffected sides, respectively. $N$ is the total number of the sample data in one gait cycle. The larger the RMS value is, the worse the gait asymmetry is.

### 6.6.2 Vertical Ground Reaction Forces

Based on the passive dynamic walking theory [17][18][19], researchers believe that the most important factors for human walking are the collision loss in the leading leg and active push-off in the trailing leg. The vertical GRFs can provide us a visual inspection on these two aspects because the second hub of the vertical GRF of the trailing leg is related to the push-off ability while the first hub of GRF of the leading leg reveals the degree of the collision lose during heel-strike. Therefore, by studying the GRFs over different experimental conditions, we can obtain an intuition on which prosthesis works better than the others.

### 6.6.3 External Work Done on the Center of Mass

Among all of the metrics, researchers believe that the most critical factor reflecting the metabolic cost consumption in bipedal locomotion is the external work done on the center of mass (COM) [17][18][19]. In particular, the total negative work performed on the COM by the leading leg represents the collision loss during heel-strike, and determines the minimum positive work need to be done by the trailing leg.

The individual limbs method, proposed in [64], was used to compute the external work done on the center of mass (COM) by each limb. In this method, the external

powers done on the COM by the trailing and leading legs were first calculated.

$$P_{trail} = \vec{F}_{trail} \cdot \vec{v}_{cm}, \tag{6.6}$$

$$P_{lead} = \vec{F}_{lead} \cdot \vec{v}_{cm}, \tag{6.7}$$

where $P_{trail}$ and $P_{lead}$ are the external power generated by the trailing and leading limbs, respectively. The positive ($W^{+}_{trail}$) and negative ($W^{-}_{trail}$) external work performed by the trailing leg were obtained by integrating the $P_{trail}$ within the positive and negative domains, or

$$W^{+}_{trail} = \int_{POS} P_{trail} dt, \tag{6.8}$$

$$W^{-}_{trail} = \int_{NEG} P_{trail} dt, \tag{6.9}$$

where $POS$ and $NEG$ are the domains in which the integrands are positive and negative, respectively. Correspondingly, the same approach was applied to calculate the positive ($W^{+}_{lead}$) and negative ($W^{-}_{lead}$) external work performed by the leading leg. The total positive ($W^{+}_{ILM}$) or negative ($W^{-}_{ILM}$) external mechanical work was obtained by summing the total positive or negative external mechanical work performed by each limb, or

$$W^{+}_{ILM} = W^{+}_{trail} + W^{+}_{lead}, \tag{6.10}$$

$$W^{-}_{ILM} = W^{-}_{trail} + W^{-}_{lead}. \tag{6.11}$$

## 6.7 Results

### 6.7.1 Basic Clinical Gait Study

During the experiments, it was discovered that the proposed finite state machine performed robustly and was capable of mimicking the target stance phase behavior. All amputee participants and the prosthetist were satisfied with the performance of the prosthesis. In general, it took less than 20 minutes for each amputee participant to adapt to the powered prosthesis. The prosthetist reported that with the powered prosthesis each participant moved with a more natural gait than with their conventional passive-elastic prosthesis. The preferred system parameters ($K_{CP}$,$K_{CD}$,$t_{pp}$,$\Delta\tau$) for each participant were recorded and are summarized in Table 6.2. Examples of the prosthesis's torque-angle behaviors for each participant are showed in Fig. 6-2. These particular parameters were used for the metabolic cost study.

### 6.7.2 Metabolic Cost Study

For each of the three experimental conditions, the steady state rate of metabolic energy consumption was determined by first plotting the total cumulative energy versus walking time for each experimental trial. The data typically reached a constant

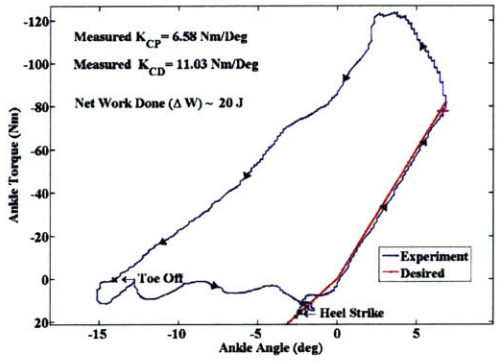


(a) Participant 1

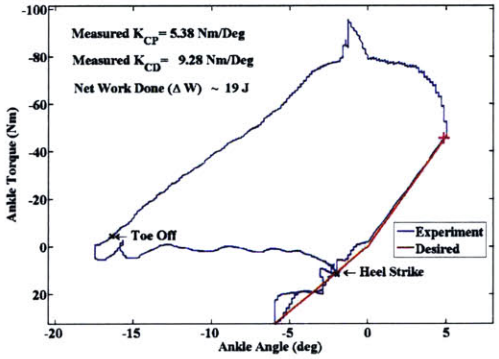


(b) Participant 2

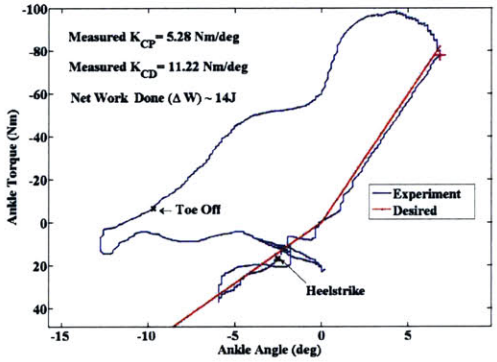


(c) Participant 3

Figure 6-2: Examples of the powered prosthesis's torque-angle behavior for each participant.

Table 6.2: Participant's Preferred System Parameters

| System Parameters | Participant | | |
|---|---|---|---|
| | 1 | 2 | 3 |
| $K_{CP}$(Nm/deg) | 6.6 | 5.4 | 3.2 |
| $K_{CD}$(Nm/deg) | 12.0 | 9.3 | 12.0 |
| $t_{pp}$(Nm) | 80 | 45 | 80 |
| $\Delta\tau$(Nm) | 90 | 90 | 65 |

Table 6.3: Results of the Metabolic Cost Study

| Results | Participant | | |
|---|---|---|---|
| | 1 | 2 | 3 |
| Walking Speed (m/s) | 1.38 | 1.67 | 1.67 |
| Net Work (J) | 20 | 19.0 | 13.7 |
| Net Work/ System Weight (J/kg) | 0.22 | 0.24 | 0.16 |
| COT (Conventional) | 0.26 | 0.25 | 0.30 |
| COT (Virtual Spring) | 0.27 | 0.23 | 0.33 |
| COT (Powered) | 0.22 | 0.20 | 0.28 |

slope after approximately 2 minutes from the start of the walking trial, indicating that the rate of metabolic energy consumption had reached a steady state value. Sample data are shown in Fig. 6-3. As can be seen, when using the powered prosthesis with nonconservative, motive power output, the participant's rate of metabolic energy consumption was the lowest among all other conditions.

The metabolic COT for each participant and experimental condition is shown in Fig. 6-4. Here again, the metabolic COT when participants used the powered prosthesis with motive power output was the lowest among all experimental conditions. The powered prosthesis with this condition was found to decrease the COT from 7% to 20% compared to the conventional passive-elastic prostheses, even though the powered system was two-fold heavier than the conventional devices. By comparing condition (3) to the virtual spring condition (2), the relative effect of the nonconservative, motive power output can be determined. The metabolic data of subject 3 show that condition (3) decreases the COT by 7% compared to condition (1) and 16% compared to condition (2), highlighting the benefits of performing net positive work during stance to amputee ambulation. The results for the metabolic COT study are summarized in Table 6.3.

### 6.7.3 Kinematics and Kinetics Study

The results of the analysis based on the proposed biomechanical metrics are shown below.

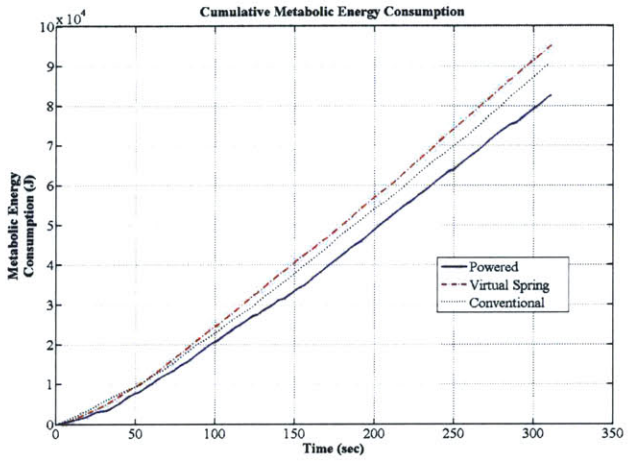


Figure 6-3: A study of metabolic energy consumption of an amputee participant walking at a self-selected speed for three conditions: (1)using their conventional passive prostheses (Conventional); (2) using the powered prosthesis with only a virtual spring response (Virtual Spring); and (3) using the powered prosthesis with a nonconservative, motive power output (Powered).

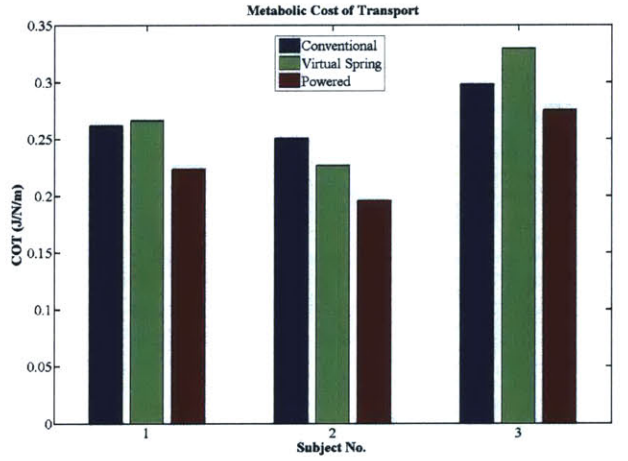


Figure 6-4: Metabolic cost of transport for three participants.

### Kinematics of Gait

An overview of kinematic data for ankle joints are shown in Fig. 6-5. Average data across all the trails and participants are shown for both affected and unaffected sides for the experimental conditions (1) and (3). The corresponding kinematics differences (RMS error) between the unaffected and affected sides for each experimental condition were computed and are shown in Fig. 6-6. The RMS error reveals that there is no significant kinematics difference in the ankle joint between the two experimental conditions.

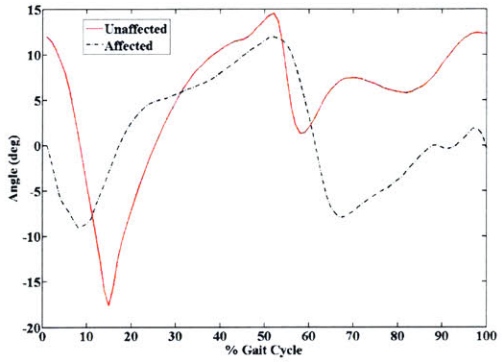


(a) Conventional

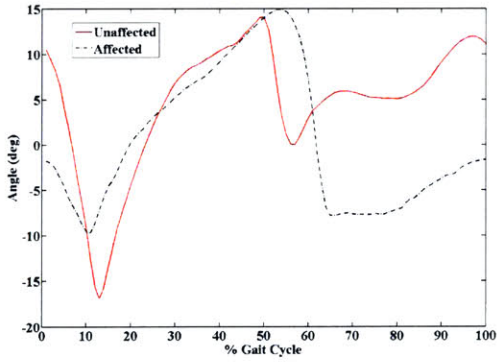


(b) Powered

Figure 6-5: Kinematics of ankle joints associated with the two experimental conditions.

### Vertical Ground Reaction Forces

Results for the comparisons of the average vertical GRFs across two conditions are shown in Fig 6-7. The powered prosthesis with motive power output was found to increase the magnitude of the second peak of the vertical GRF by 36%, compared to the conventional prosthesis. Furthermore, it also slightly lowers the first peak's magnitude of the GRF for the leading leg (unaffected side) by about 8%, compared

to the conventional prosthesis. This indicates a slight reduction of the impact loss in the leading leg.

### External Work Done on the Center of Mass

Results for the comparisons of the external work done on COM by each limb across two conditions are shown in Fig. 6-8. Using powered prosthesis with motive power output, the $W^{-}_{lead}$ decreased by 22% and $W^{+}_{trail}$ increased by 6%, as compared to the conventional prosthesis. Both the $W^{-}_{trail}$ and $W^{+}_{lead}$ were not discussed here because they are insignificant when compared to $W^{-}_{trail}$ and $W^{+}_{trail}$ [63][64].

## 6.8 Discussion

Although researchers have anticipated that an ankle-foot prosthesis providing non-conservative, motive power output may improve amputee walking economy, no one has successfully developed a high performance powered ankle-foot prosthesis to verify this hypothesis. In this thesis, I investigate this hypothesis using the proposed control system in a novel powered ankle-foot prosthesis. The metabolic results shown in this chapter support this hypothesis. When using the powered ankle with motive power output, the metabolic COT for the tested subjects decreases by 7% to 20%, compared to their conventional passive-elastic prostheses, even though the powered system was two-fold heavier than the conventional devices.

Furthermore, the results of the vertical GRF and the ankle torque-angle characteristics for the affected side demonstrate the energetic differences between the conventional (Condition (1)) and the powered prostheses (Condition (3)). Most notably, the powered prosthesis provides a significant large net positive work, which is not available in the conventional prosthesis. It is reasonable to anticipate that this extra amount of positive work may compensate part of the energy loss in walking for the redirection of the center of mass velocity during step-to-step transitions [17][18][19]. Consequently, the amputee participants need to exert less energy for walking. This may be one reason for the reduction in walking metabolic cost for the participants.

Just by inspecting the results in Figs. 6-5 and 6-6, it is hard to conclude that the powered prosthesis can improve the gait kinematics symmetry of amputee participants. The difficulty in assessing the gait symmetry would seem to stem from not providing enough time for the amputee participants to acclimatize to the powered prosthesis. To better address this issue, the experimental protocol may need to be modified to allow each participant to use the prosthesis for a few days before measuring the kinematics data. One thing we can conclude is that the reduction in the metabolic walking economy of the amputee participants is probably not a consequence of the improvement of the kinematics symmetry.

Finally, I hypothesize that the powered prosthesis with motive power output reduces the negative work done on the COM by the trailing leg ($W^{-}_{trail}$), compared to the conventional prosthesis. The kinetic study supports this hypothesis. With the powered prosthesis with motive power output, $W^{-}_{trail}$ decreases by 22% compared to

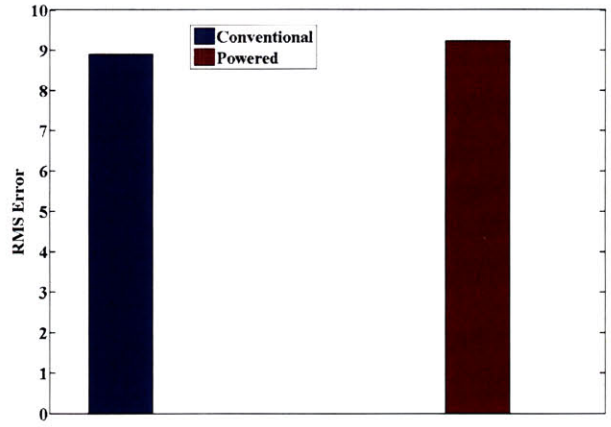


Figure 6-6: Kinematics differences of the ankle joint between the affected and unaffected sides for the two experimental conditions.

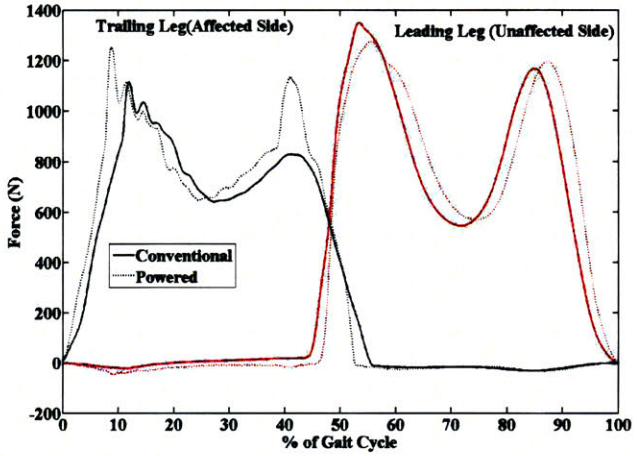


Figure 6-7: Average vertical ground reaction forces for both leading and trailing legs over one gait cycle. The powered prosthesis with motive power output significantly increased the magnitude of the second peak of normal force of the trailing leg. It also slightly lowered the first peak's magnitude of the normal force in the leading leg, i.e. less impact loss occurred in the leading leg.

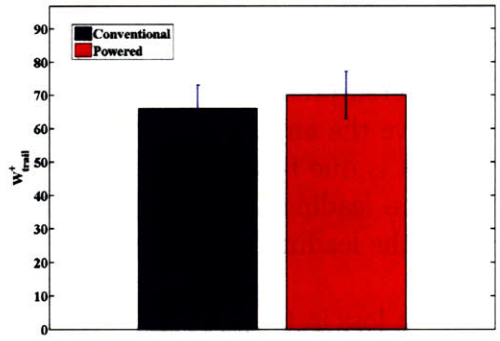


(a) Positive work done on the COM by the trailing leg ($W^{+}_{trail}$)

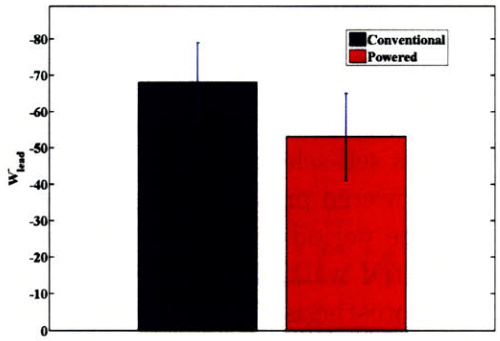


(b) Negative work done on the COM by the leading leg ($W^{-}_{lead}$)

Figure 6-8: Comparisons of the external work done on the COM by each limb for two experimental conditions

the conventional prosthesis. According to the literature, $W^{-}_{trail}$ is the determinant of the energy loss in walking due to the redirection of the center of mass velocity during step-to-step transitions [17][18][19]. The smaller the $W^{-}_{trail}$ is, the less the metabolic cost is required for walking. The reduction in $W^{-}_{trail}$ may provide an explanation for the metabolic cost reduction for the amputee participants.

In summary, the results of the initial clinical evaluation indicate that the proposed design and control of the powered ankle-foot prosthesis has significant advantages over conventional passive-elastic prostheses for unilateral amputees walking at self-selected speeds. In the remainder of this section, I further discuss biomechanical mechanisms for the metabolic cost reduction associated with the powered prosthesis. Then, I discuss some initial findings on the increase in self-selected walking speed of the amputee subject using the powered prosthesis. Finally, I provide the participants' comments on the proposed prosthesis.

### 6.8.1 Biomechanical Mechanisms for Metabolic Cost Reduction

The results show that the powered prosthesis with a non-conservative motive power output can significantly improve the amputee participants' walking metabolism. As mentioned, one possible reason is due to the reduction in the negative work ($W^{-}_{lead}$) performed on the COM by the leading leg (unaffected side), i.e. less impact loss occurred during heel-strike of the leading leg. The kinetics study has supported this hypothesis.

Besides reducing the impact loss in the unaffected side, another possible explanation is that the powered prosthesis reduces the net work done by the hip joints of the amputee, causing the reduction in the metabolic cost of walking. Unfortunately, the kinetics data for the hip and knee joints are not available in this thesis, therefore, no data can be used to support or evaluate this hypothesis.

### 6.8.2 Increase in Self-Selected Walking Speed

As mentioned in Section 1, researchers have hypothesized that a powered prosthesis may also increase an amputee's self-selected walking speed [17][18][19]. Throughout the clinical evaluation of the powered prosthesis, we observed that the amount of net positive work during the stance period does have an effect on self-selected walking speed. For example, self-selected walking speed was increased with participant 2. Using his conventional passive prosthesis, his self-selected speed was 1.45m/s, whereas with the powered prosthesis, his self-selected speed was increased to 1.68 m/s, a 16% increase in forward speed. It is noted here that when using the powered ankle-foot prosthesis, not only was this participant's walking speed increased by 16%, but his COT was still 10% lower than when he used the conventional prosthesis at the slower 1.45 m/s speed(see Fig. 6-9).

### 6.8.3 Prosthesis Weight Versus Power Output

Due to the passive nature of conventional prostheses, and their relatively low power output capability, prosthetic designers have sought to keep prosthetic weight much less than that of the human ankle-foot complex in an effort to maximize walking metabolic economy. This investigation demonstrated improvement in amputee walking economy with the powered ankle-foot prosthesis. This result highlights the fact that prosthesis weight is not necessarily a detriment to the clinical performance of a prosthetic intervention. Clearly, the weight of a powered ankle-foot prosthesis may not hinder an amputee's gait as long as the prosthesis can provide sufficient power output at terminal stance.

### 6.8.4 Participants' Comments

All amputee participants were satisfied with the performance of the prosthesis. They reported that the powered prosthesis did not feel heavy when the motive power con-

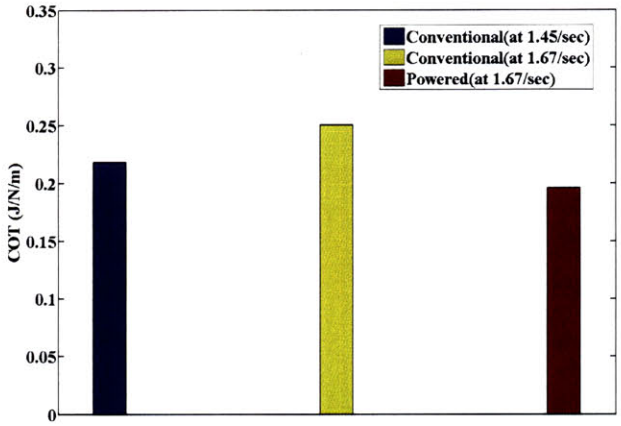


Figure 6-9: Comparisons of the metabolic cost of transport for participant 2 for different walking speeds.

troller was employed (condition 3). They also expressed that the powered prosthesis with the motive power controller made walking easier and less demanding as compared to the conventional passive prostheses evaluated in the study. Not surprisingly the participants reported that the powered prosthesis felt exceedingly heavy when the virtual spring controller was used (condition 2). They also believed that if they were allowed to practice with the powered prosthesis for couples more day, they could perform better with the prosthesis.

# Chapter 7

# Conclusions and Future Work

## 7.1 Thesis Contributions

According to Section 1.2, two major engineering challenges hinder the development process of a powered ankle-foot prosthesis: First, it is challenging to build an ankle-foot prosthesis that matches the size and weight of the intact ankle, while providing sufficiently large instantaneous power output and torque to propel an amputee. Second, it is unclear what kind of prosthetic control strategy is effective for the improvement of amputee gait.

The work accomplished in this thesis has (i) demonstrated the feasibility of developing a powered ankle-foot prosthesis; (ii) proposed and implemented an effective control scheme for the improvement of amputee ambulation; and (iii) demonstrated improvement in amputee walking economy with the powered ankle-foot prosthesis based on the clinical evaluation. These contributions can be further elaborated as follows:

- **Mechanical design and analysis**

  This thesis proposes a new design architecture for a powered ankle-foot prosthesis to overcome force bandwidth challenges. The novel architecture comprises a unidirectional spring, configured in parallel with a force-controllable actuator with series elasticity. With this configuration, the powered prosthesis provides a sufficiently high mechanical power output (or large force bandwidth) and a large peak torque within the weight and size constraints of an ankle-foot prosthesis. The basic architecture of parallel and series elasticity may also prove useful for other types of assistive devices that require both high power and torque output, such as a hip-actuated orthosis [59].

  Furthermore, in this thesis, I conducted several basic steady-state and dynamic analyses to evaluate the intrinsic mechanical performance of the system. These analyses were essential to guide the selections of system components. Working in collaboration with Jeff Weber, a mechanical designer, we designed and built a physical prototype of the powered ankle-foot prosthesis, called MIT Powered Ankle-Foot Prosthesis. In addition, once the ankle-foot system was constructed, I conducted experiments to characterize the actual system behavior.

- **Control system design**

  Motivated by human ankle walking mechanics, I proposed a stance phase control scheme that mimicks the quasi-static stiffness behavior and power generation characteristics of the human ankle during steady state walking.

  To realize the scheme, I first developed three basic low-level servo controllers, including a high performance force controller, an impedance controller, and a position controller. In particular, the high performance force controller attempts to provide a sufficiently high force output and bandwidth for the active push-off, by utilizing the displacement feedback of the series spring.

  Furthermore, I proposed a finite-state controller to provide the target stance phase behavior. Finally, I implemented the controller on the MIT Powered Ankle-Foot Prosthesis and clinically evaluated controller performance with amputee subjects. The results of the basic gait study showed that the proposed finite state machine performed robustly and was capable of mimicking the target stance phase behavior.

- **Clinical evaluation**

  To evaluate the influence of the prosthesis on amputee walking, I first conducted a basic gait study on three unilateral amputees. All participants and their prosthetist were satisfied with the performance of the prosthesis. The amputee participants reported on a relatively fast adaptation period ($<$ 20 mins). The prosthetist reported that each participant moved with a more natural gait with the powered prosthesis than with their conventional passive-elastic prosthesis.

  I then estimated the metabolic power requirements of the amputee participants while walking with the powered prosthesis and a passive-elastic conventional prosthesis. When using the powered prosthesis, the metabolic COT was shown to decrease by 7% to 20%, as compared to their conventional passive-elastic prostheses, even though the powered system was two-fold heavier than the conventional devices. For one study participant, walking speed increased by 16% when using the powered prosthesis, but the COT was still 10% lower than when the participant used the conventional prosthesis at the slower speed.

  Finally, I conducted a kinematics and kinetics study on one of the amputee participants. Initial results show that the powered prosthesis reduces the negative mechanical work performed by the leading biological leg during double support, lowering impact losses. This may explain the metabolic cost reduction associated with the powered prosthesis.

## 7.2 Future Work

### 7.2.1 A Comprehensive Biomechanical Gait Study

The measured metabolic cost reduction associated with the powered prosthesis is very compelling evidence in support of our hypothesis. Yet additional kinematic and

kinetic data from more amputee subjects will be necessary to provide a more solid explanation for the underlying biomechanical mechanism for the observed metabolic reduction. Furthermore, the study may also shed new lights on the optimal control design of a powered ankle-foot prosthesis.

### 7.2.2 Further improvements to the Powered Ankle-Foot Prosthesis

Before the MIT Powered Ankle-Foot Prosthesis can be ready for general use by the amputee population, several hardware improvements are necessary. First, the current prototype used in this investigation is still too heavy and power intensive to be practical for general amputee use. More importantly, it is necessary to reduce the size (low profile) of the prosthesis so that more amputee users can use the prosthesis. Second, the electronics and computing platform using in the investigation need to be miniaturized into a small PCB integrated into the prosthesis. Third, the power source should be seated next to the prosthesis, so that the amputee need not wear a backpack loaded with battery.

Researchers in the Biomechatronics Group at MIT Media Lab have conducted an initial attempt to develop a more viable prototype ankle-foot prosthesis(See Fig. 7-1). The design of the prosthesis fits both human foot/ankle dimensions and geometry, with compact integrated battery and other electronic components.

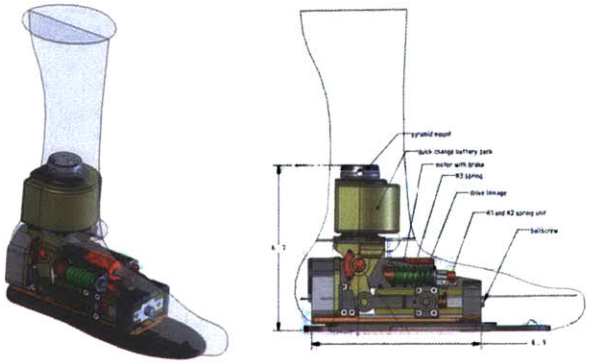

Figure 7-1: A more viable prototype ankle-foot prosthesis. The ankle design includes an electric motor and a motor series spring. In parallel with the motor is an electromagnetic brake. A uni-directional spring is engaged for ankle angles of 90 degrees or less (dorsiflexion). The design is shown superimposed within a scan of a human foot and ankle to demonstrate that it is in the proper form factor.

# Appendix A

# Subject Consent Forms

Biomechatronics Group
MIT Media Laboratory
Active Ankle-Foot Prosthesis Study
Consent Form for Subjects with Below-knee Amputation

You are invited to participate in a research study conducted by Dr. Hugh Herr, Ph.D., Mr. Samuel K. Au, B.S.E, Ernesto C. Martinez, B.S.E, and Lee Magnusson, B.S.E, from the Biomechatronics Group, MIT Media Laboratory at the Massachusetts Institute of Technology (M.I.T.). You will be invited to be a participant in this study. You should read the information below, and ask questions about anything you do not understand before deciding whether or not to participate.

## PARTICIPATION AND WITHDRAWAL

Your participation in this research is completely VOLUNTARY. If you choose to participate you may subsequently withdraw from the study at any time without penalty or consequences of any kind. If you choose not to participate, that will not affect your relationship with M.I.T. or your right to health care or other services to which you are otherwise entitled or will not cause you to lose your research compensation.

## PURPOSE OF THE STUDY

The purpose of this study is to develop an active ankle-foot prosthetic device for below-knee amputees. Commercially available ankle-foot prostheses are completely passive, and consequently, their mechanical properties remain fixed with walking speed and terrain. This new active ankle-foot prosthesis will mimic the behaviours of the normal human ankle during walking and also adapt to your walking speed. This active prosthesis has been tested in a previous study, and has the potential for increasing gait symmetry and walking economy of a below-knee amputee.

## DEVICE DETAILS

The active ankle-foot prosthesis will comprise a series-elastic actuator (SEA) and a elastic leaf spring, previously developed for robotic and human rehabilitation applications. The SEA will allow for precise force control of the ankle joint, mimicking the spring-like behavior of the human ankle, as well as providing adequate energy for forward progression of the body. From the early stance period to the mid-stance period, the SEA will be controlled in a way that the ankle joint behaves like a spring. In the late stance period, the SEA will be employed to power the forward movement of the body. The elastic leaf spring will provide shock absorption during foot strike, energy storage during early stance, and energy return during late stance.

## PROCEDURES

The complete study will include three separate experimental sessions conducted in three different locations. These locations are: The Biomechatronics Group, MIT Media Laboratory (E15-054), the Holodeck room in CSAIL at MIT (Rm 33-339), and the Indoor Track at MIT's Johnson Athletic Center. The time among experimental sessions will be approximately one to two weeks and the time duration of each session will be two to three hours. For each session, you will be asked to walk at slow, normal, and fast paces for three different conditions. The experimental conditions are:

1. Using an assigned commerically, available below-knee prosthesis
2. Using the active prosthesis with a virtual spring program (In this condition, the prosthesis will be programmed as a spring-like behavior.)
3. Using the active prosthesis with the motive power program (In this condition, the prosthsis will be programmed as a spring-like behavior with an additional push-off for forward propulsion.)

We will also take measurements to determine the length of your limbs and your body weight in each session.

In the first session, you will be scheduled to visit the Biomechatronics Group in The Media Laboratory at MIT. The main purpose of this session is to qualitatively assess the degree to which the active prosthesis can improve gait symmetry and walking economy. You will be asked to walk along a 30-foot level walkway in the Biomechatronics Group. During the session, you will be asked to walk at slow, normal and fast paces for each of three walking conditions. For each condition and speed, approximately 10-15 trials will be performed. Parallel bars will be utilized to prevent any injury to you in the event that you lose your balance and fall. A safely harness attached to the ceiling will also be utilized if you request for. In addition, a member of the laboratory staff will accompany you, if necessary. You may ask to rest or stop the study at any time. You will be walking on the platform 60-90 times for the entire first session, which should take 2 hours. When using the active prosthesis with the walking program, our researchers will tune the parameters of the program to match your own gait pattern.

In the second session, you will be scheduled to visit the Holodeck room in CSAIL at MIT (Rm 33-339),that has installed the motion capture system to measure human

movement. The main purpose of this session is to quantitatively assess the degree to which the active prosthesis can improve gait symmetry and walking economy. You will be asked to walk along a 30-foot level walkway in the Holodeck room in CSAIL at MIT. Before conducting experiments, one of the investigators will place reflective markers on the your skin with tape at specific points over joints of your body. These special markers are then seen by the cameras in the room. During the session, you will be asked to walk at slow, normal and fast paces for each of three walking conditions. For each condition and speed, approximately 10-15 trials will be performed. Motion data is collected from cameras in the room and from the forceplaces, that are placed in the walkway. As the device has been setup in the first session, two members of the laboratory staff will walk on each side of you throughout the experiment.

In the third session, you will be scheduled to visit the Indoor Track of the Johnson Athletic Center at MIT, which is located on the 2nd floor of the Athletic Center. The main purpose of this session is to test if the active ankle-foot prosthesis does, in fact, reduce the metabolic cost of amputee walking. During the session, you will be asked to wear a Cosmed Oxygen Consumption (VO2) mask that will measure the rate with which you consume oxygen and will determine your metabolic rate. Two hours prior to testing, you will be asked not to eat. As the device has been setup in the first session, two members of the laboratory staff will walk on each side of you throughout the experiment. The procedure will be as follows:

You will wear the VO2 system and first walk for 8 minutes on the track with an assigned commercially, available below-knee prosthesis to establish a control metabolic rate. After resting for 8 minutes, you will wear the active prosthesis with virtual spring program and get acclimated to the device by walking for 5 minutes. You will then walk on the track for 8 minutes as we measure your metabolic rate with the device. You will then rest for another 8 minutes. After resting, the active prosthesis will be turned on with the motive power program. You will get acclimated to the device by walking for 5 minutes. You will then walk on the track for another 8 minutes as we measure your metabolic rate with the device. This protocol will be repeated two additional times, and the entire experiment will take approximately 3 hours.

Throughout the study, you will be videotaped and photographed to document the effect of the prosthesis on walking. Sensor data from the prosthesis will be captured and that muscular activity will be recorded via surface electrodes. You may be asked to return for optional sessions, just in case more data are needed to evaluate the prosthesis that we are building.

## POTENTIAL RISKS AND DISCOMFORTS

1. As with any prosthetic walking, there is a small risk of falling during the trials. This will be minimized by having parallel bars in the Biomechatronics Group. If necessary, a safety harness attached to the ceiling can also be provided. In the second session, although there is no parallel bars and safety harness provided for you, we will assign two assistants walk on each side of you.

2. The electronics will have two kill switches, one on the operator and one remote so that either the subject or the investigator can immediately disable the device.

3. Since the active prosthesis is an active device, there is a risk of malfunction. The developers will make every effort to reduce this risk, but if a malfunction occurs, the prosthesis will default to a inactive state where it will become rigid, like a standard ankle-foot prosthesis. Also, you will have standard parallel bars to catch you. If you fail to catch yourself with the parallel bars, the assistant walking beside you will also hold you upright.

4. If you become too fatigued, you may ask to rest or stop the study at any time.

5. As with any prosthetic device, there is also potential physical discomfort from wearing the prosthesis.

6. This device is investigational and there may be risks and side effects that are currently unknown and/or unanticipated.

## ANTICIPATED BENEFITS TO SUBJECTS

You should not expect your ambulation to improve as a result of participating in this research.

## ANTICIPATED BENEFITS TO SOCIETY

1. Development of an active ankle foot prosthesis that may help below-knee amputees walk with a more normal gait. 2. There are no known direct benefits for participating in this experiment. The prosthesis being developed is a prototype and will not be immediately available.

## ALTERNATIVES TO PARTICIPATION

The alternative to participating in this study is to continue with your regular treatment under the direction of your primary care physician.

## PAYMENT FOR PARTICIPATION

You will receive a stipend of 10 dollars per hour to compensate for your time, effort and travel expenses. We will assist in arranging your transportation but cannot pay transportation cost.

## POSSIBLE COMMERCIAL PRODUCTS

The prosthesis may become a commercial prosthetic device for below-knee amputees.

## FINANCIAL OBLIGATION

Neither you nor your insurance company will be billed for your participation in this research.

## PRIVACY AND CONFIDENTIALITY

The only people who will know that you are a research participant are members of the research team and, if appropriate, your physicians and nurses. No information about you, or provided by you during the research will be disclosed to others without your written permission, except: if necessary to protect your rights or welfare, or if required by law.

When the results of the research are published or discussed in conferences, no information will be included that would reveal your identity. If photographs, videos, or audio-tape recordings of you will be used for educational purposes, your identity will be protected or disguised. The videotapes and photos will be under the control of the MIT Media Laboratory's Biomechatronics Group. After the results are published, a copy of the photos and videos will be kept on file in the laboratory for future reference.

## WITHDRAWAL OF PARTICIPATION BY THE INVESTIGATOR

The investigator may withdraw you from participating in this research if circumstances arise which warrant doing so. If you experience any side effects or if you become ill during the research, you may have to drop out, even if you would like to continue. The investigator, Hugh Herr, will make the decision and let you know if it is not possible for you to continue. The decision may be made either to protect your health and safety, or because it is part of the research plan that people who develop certain conditions may not continue to participate.

If you must drop out because the investigator asks you to or because you have decided on your own to withdraw, you will still receive the travel compensation.

## NEW FINDINGS

During the course of the study, you will be informed of any significant new findings (either good or bad), such as changes in the risks or benefits resulting from participation in the research or new alternatives to participation that might cause you to change your mind about continuing in the study. If new information is provided to you, your consent to continue participating in this study will be re-obtained.

## EMERGENCY CARE AND COMPENSATION FOR INJURY

In the unlikely event of physical injury resulting from participation in this research, you may receive medical treatment from the M.I.T. Medical Department, including emergency treatment and follow-up care as needed. Your insurance carrier may be billed for the cost of such treatment. M.I.T. does not provide any other form of

compensation for injury. Moreover, in either providing or making such medical care available it does not imply the injury is the fault of the investigator. Further information may be obtained by calling the MIT Insurance and Legal Affairs Office at 1-617-253 2822.

## IDENTIFICATION OF INVESTIGATORS

In the event of a research related injury or if you experience an adverse reaction, please immediately contact one of the investigators listed below. If you have any questions about the research, please contact Hugh Herr at (617) 258-6574 or at Building E15, Room 419, 20 Ames Street, Cambridge, MA.

## RIGHTS OF RESEARCH SUBJECTS

You are not waiving any legal claims, rights or remedies because of your participation in this research study. If you feel you have been treated unfairly, or you have questions regarding your rights as a research subject, you may contact the Chairman of the Committee on the Use of Humans as Experimental Subjects, M.I.T., Room E32-335, 77 Massachusetts Ave, Cambridge, MA 02139, phone 1-617-253 6787.

## SIGNATURE OF RESEARCH SUBJECT OR LEGAL REPRESENTATIVE

I have read (or someone has read to me) the information provided above. I have been given an opportunity to ask questions and all of my questions have been answered to my satisfaction. I have been given a copy of this form.

**BY SIGNING THIS FORM, I WILLINGLY AGREE TO PARTICIPATE IN THE RESEARCH IT DESCRIBES.**

_____

Name of Subject

_____

Name of Legal Representative (if applicable)

_____ _____

Signature of Subject or Legal Representative Date

## SIGNATURE OF INVESTIGATOR

I have explained the research to the subject or his/her legal representative, and answered all of his/her questions. I believe that he/she understands the information described in this document and freely consents to participate.

_____

Name of Investigator

_____ _____

Signature of Investigator Date (must be the same as subject's)

**SIGNATURE OF WITNESS (If required by COUHES)**

My signature as witness certified that the subject or his/her legal representative signed this consent form in my presence as his/her voluntary act and deed.

_____

Name of Witness

_____ _____

Signature of Witness Date

# Bibliography


[1] www.ossur.com.

[2] S. Ron, *Prosthetics and Orthotics: Lower limb and Spinal.* Lippincott Williams & Wilkins, 2002.

[3] N. H. Molen, "Energy/speed relation of below-knee amputees walking on motor-driven treadmill," *Int. Z. Angew. Physio,* Vol. 31, pp.173, 1973.

[4] G. R. Colborne, S. Naumann, P. E. Longmuir, and D. Berbrayer, "Analysis of mechanical and metabolic factors in the gait of congenital below knee amputees," *Am. J. Phys. Med. Rehabil.,* Vol. 92, pp. 272 - 278, 1992.

[5] R. L. Waters, J. Perry, D. Antonelli, H. Hislop. "Energy cost of walking amputees: the influence of level of amputation," *J Bone Joint Surg. Am.,* Vol. 58, No. 1, pp. 4246, 1976.

[6] D. A. Winter and S. E. Sienko, "Biomechanics of below-knee amputee gait," *Journal of Biomechanics,* Vol. 21, No. 5, pp. 361-7, 1988.

[7] H. B. Skinner and D. J. Effeney, "Gait analysis in amputees," *Am J Phys Med,* Vol. 64, pp. 82-89, 1985.

[8] H. Bateni and S. Olney, "Kinematic and kinetic variations of below-knee amputee gait," *Journal of Prosthetics & Orthotics,* Vol. 14, No. 1, pp. 2- 13, 2002.

[9] K. Koganezawa, and I. Kato, "Control aspects of artificial leg," *IFAC Control Aspects of Biomedical Engineering*, pp.71-85, 1987.

[10] D. A. Winter, "Biomechanical motor pattern in normal walking," *Journal of Motor Behavior*, Vol. 15, No. 4, pp. 302 - 330, 1983.

[11] M. Palmer, "Sagittal plane characterization of normal human ankle function across a range of walking gait speeds," *Master's Thesis,* Massachusetts Institute of Technology, 2002.

[12] D. H. Gates, "Characterizing ankle function during stair ascent, descent, and level walking for ankle prosthesis and orthosis design," *Master's thesis,* Boston University, 2004.

[13] R. B. Davis and P. A. Deluca, "Gait characterization via dynamic joint stiffness," *Gait & Posture,* Vol. 4, pp. 224-23, 1996.

[14] A. Hansen, D. S. Childress, S. C. Miff, S. A. Gard, K. P. Mesplay, "The human ankle during walking: implication for the design of biomimetric ankle prosthesis," *Journal of Biomechanics,* Vol. 37, Issue 10, pp. 1467-1474, 2004.

[15] A. L. Hof, B. A. Geelen, J. Van den Berg, "Calf muscle moment, work and efficiency in level walking; role of series elasticity," *Journal of Biomechanics,* Vol. 16, No. 7, pp. 523-537, 1983.

[16] A. D. Kuo, "A simple model of bipedal walking predicts the preferred speed-step length relationship," *Journal of Biomechanical Engineering,* Vol. 123, pp. 264-269, 2001.

[17] A. D. Kuo, "Energetics of actively powered locomotion using the simplest walking model," *Journal of Biomechanical Engineering,* Vol. 124, pp. 113-120, 2002.

[18] A. D. Kuo, J. M. Donelan, and A. Ruina, "Energetic consequences of walking like an inverted pendulum: Step-to-step transitions," *Exercise and Sport Sciences Reviews,* Vol. 33, pp. 88-97, 2005.

[19] A. Ruina, J. E. Bertram, and M. Srinivasan, "A collisional model of the energetic cost of support work qualitatively explains leg sequencing in walking and galloping, pseudo-elastic leg behavior in running and the walk-to-run transition," *Journal of Theoretical Biology,* Vol. 237, Issue 2, pp. 170-192, 2005.

[20] G. K. Klute, J. Czerniecki, and B. Hannaford, "Development of powered prosthetic lower limb," *Proc. 1st National Mtg,* Veterans Affairs Rehab. R&D Service, Washington, DC, October 1998.

[21] S. H. Collins and A. D. Kuo, "Controlled energy storage and return prosthesis reduces metabolic cost of walking," *Proc. on ISB XXth Congress and the American Society of Biomechanics Annual Meeting,* Cleveland, Ohio, pp. 804, August 2003.

[22] C. Li, T. Miwa , J. Furusho, S. Morimoto, K. Koyanagi, A. Nakagawa, Yasushi-Akazawa, and Y. Hashimoto,"Research and development of the intelligently-controlled prosthetic ankle joint," *Proc. of IEEE Int. Conf. on Mechatronics and Automation,* Luoyang, China, pp. 1114-1119, 2006.

[23] US Patent 6443993, Sept. 3, 2002.

[24] V. T. Inman, H. J. Ralston, and F. Todd, *Human walking.* Baltimore: Williams and Wilkins; 1981.

[25] J. Perry, *Gait Analysis: Normal and Pathological Function.* New Jersey: SLACK Inc.; 1992.

[26] S. K. Au, J. Weber, and H. Herr, "An ankle-foot emulator system for the study of human walking biomechanics," *Proc. IEEE Int. Conf. on Robotics and Automation,* Orlando, FL, pp. 2939-2945, May 2006.

[27] K. Hirai, M. Hirose, Y. Haikawa, and T. Takenaka,"The development of Honda humanoid robot," *Proceedings on IEEE/RSJ International Conference on Intelligent Robots and Systems,* Leuven, Belgium, pp. 1321-1326, May 1998.

[28] K. Kaneko, et. al., "Humanoid robot HRP-2," *Proc. IEEE Int. Conf. on Robotics and Automation,* New Orleans, LA, pp. 1083-1090, April 2004.

[29] S. Mochon and T. A. McMahon, "Ballistic walking," *Journal of Biomechanics,* Vol. 13, pp.49-57, 1980.

[30] F. C. Anderson and M. G. Pandy, "Dynamic optimization of human walking," *Journal of Biomechanical Engineering,* Vol. 123, pp.381-390, 2001

[31] R. McN. Alexander, "Simple models of human motion," *Appl. Mech. Rev.,* Vol. 48, pp. 461-469, 1995.

[32] D. A. Winter, "Energy generation and absorption at the ankle and knee during fast, natural, and slow cadences," *Clinical Orthopedics and Related Research,* Vol. 175, pp. 147-154, 1983.

[33] D. A. Winter, *The Biomechanics and Motor Control of Human Gait.* Waterloo, Ontario: University of Waterlo; 1987.

[34] D. H. Nielsen, D. G. Shurr, J. C. Golden, and K. Meier, "Comparison of energy cost and gait efficiency during ambulation in below-knee amputees using different prosthetic feet - a preliminary report," *Journal of Prosthetics & Orthotics,* Vol. 1, No. 1, pp. 24-29, 1989.

[35] P. A. Macfarlane, D. H. Nielsen, D. G. Shurr, and K. Meier, "Gait comparisons for below-knee amputees using a flex-foot versue a conventional prosthetic foot," *Journal of Prosthetics & Orthotics,* Vol. 3, No. 4, pp. 150-159, 1991.

[36] D. G. Barth, L. Schumacher, and S. Sienko, "Gait analysis and energy cost of below-knee amputees wearing six different prosthetic feet," *Journal of Prosthetics & Orthotics,* Vol. 4, No. 2, pp. 63-72, 1992.

[37] J. Perry and S. Shanfield, "Efficiency of dynamic elastic response prosthetic feet," *Journal of Rehabilitation Research and Development,* Vol. 30, No. 1, pp. 137-143, 1993.

[38] J. F. Lehmann, R. Price, S. Boswell-Bessette, A. Dralle, and K. Questad, "Comprehensive analysis of dynamic elastic response feet: Seattle Ankle/Lite Foot versus standard SACH Foot," *Arch Phys Med Rehabil,* Vol. 74, pp. 853861, 1993.

[39] J. M. Casillas, V. Dulieu, M. Cohen, I. Marcer, and J. P. Didier, "Bioenergetic comparison of a new energy-storing foot and SACH foot in traumatic below-knee vascular amputations," *Arch Phys Med Rehabil*, Vol. 76, No. 1, pp. 3944, 1995.

[40] G. K. Klute, C. F. Kallfelz, J. M. Czerniecki, "Mechanical properties of prosthetic limbs adapting to the patient," *Journal of Rehabilitation Research and Development,* Vol. 38, No. 3, pp. 299-307, 2001.

[41] G. A. Pratt and M. M. Williamson, "Series elastic actuators," *Proceedings on IEEE/RSJ International Conference on Intelligent Robots and Systems,* Pittsburgh, pp.399-406, 1995.

[42] D. Robinson, "Design and an analysis of series elasticity in closed-loop actuator force control," *Ph.D. Thesis,* Massachusetts Institute of Technology, 2000.

[43] S. K. Au, J. Weber, and H. Herr, "Biomechanical design of a powered ankle-foot prosthesis," Accepted by ICORR 2007.

[44] www.maxon.com

[45] C. T. Johnson and R. D. Lorenz, "Experimental identification of friction and its compensation in precise, position controlled mechanisms," *IEEE Trans. on Industry Applications,* Vol. 28, No. 6, pp. 1392-1398.

[46] D. Paluska and H. Herr, "The effect of series elasticity on actuator power and work output: implications for robotic and prosthetic joint design," *Robotics and Autonomous Systems*, Vol. 54, pp. 667-673, 2006.

[47] K. W. Hollander, T. G. Sugar, and D. E. Herring, "Adjustable robotic tendon using a 'Jack Spring'$^{TM}$," *Proceedings on IEEE International Conference on Rehabilitation Robotics,* Chicago, pp. 113-118, 2005.

[48] S. D. Eppinger and W. P. Seering, "Three dynamic problems in robot force control," *IEEE Transactions on Robotics and Automation,* Vol. 8, No. 6, pp. 751-758, 1992.

[49] N. Hogan, "Impedance control: an approach to manipulation: Part I-III," *AMSE J. Dynamic Syst. Meas. Control,* Vol. 107, pp. 1-24, 1985.

[50] N. Hogan and S. P. Buerger, "Impedance and Interaction Control," *Robotics and Automation Handbook,* CRC Press, pp. 19.1-19.24, 2005.

[51] K.A. Pasch and W. P. Seering, "On the drive systems for high performance machines," *AMSE J. Mechanisms, Transmissions, and Automation in Design* Vol. 106, pp. 102-108, 1984.

[52] N. Hogan and S. P. Buerger, "Impedance and Interaction Control," Chapter 19 in: *Robotics and Automation Handbook*, T.R.Kurfess, (ed.) CRC Press; 2004.

[53] J. E. Colgate, "The control of dynamically interaction systems," Massachusetts Institute of Technology, *Ph.D. Thesis,* 1998.

[54] D. L. Grimes, "An active multi-mode above-knee prosthesis controller," *Ph.D. Thesis,* Massachusetts Institute of Technology, 1976.

[55] D. Zlatnik, B. Steiner, and G. Schweitzer, "Finite-state control of a trans-femoral prosthesis," *IEEE Trans. on Control System Technology,* Vol. 10, No. 3, pp. 408-420.

[56] A. J. Wilkenfeld, "Biologically inspired auto adaptive control of a knee prosthesis," *Ph.D. Thesis,* Massachusetts Institute of Technology, 2000.

[57] J. A. Blaya and H. Herr, "Adaptive control of a variable-impedance ankle-foot orthosis to assist drop-foot gait," *IEEE Transactions on Neural Systems and Rehabilitation Engineering,* Vol. 12, No. 1, pp. 24-31, 2004

[58] www.mathworks.com

[59] C. J. Walsh, "Biomimetic Design of an Under-Actuated Leg Exoskeleton For Load-Carrying Augmentation," *Master's Thesis,* Massachusetts Institute of Technology, 2006.

[60] H. Geyer, A. Seyfarth, and R. Blickhan, "Positive force feedback in bouncing gaits," *Proceeding of Royal Society of London in Biological Sciences,* Vol. 270, No. 1529, pp. 2173-2183, 2003.

[61] C. Hausswirth, A.X. Bigard, and J.M. Lechevelier, "The Cosmed K4 telemetry system as an accurate device for oxygen uptake measurement during exercise," *Int. J. of Sports Medicine,* Vol. 18, pp.449-453, 1997.

[62] J.M. Brockway, "Derivation of formulae used to calculate energy expenditure in man," *Human Nutrition: Clinical Nutrition,* Vol. 41, pp. 463-471, 1987.

[63] J. M. Donelan, R. Kram, and A. D. Kuo, "Mechanical work for step-to-step transitions is a major determinant of the metabolic cost of human walking," *J. Exp. Biol.,* 205, pp. 3717-3727, 2002.

[64] J. M. Donelan, R. Kram, and A. D. Kuo, "Simultaneous positive and negative external work in human walking," *Journal of Biomechanics,* 35, pp. 117-124, 2002.

[65] J. L. Johansson et al., "A clinical comparison of variable damping and mechanically passive prosthetic knee devices," *American Journal of Physical Medicine & Rehabilitation,* Vol. 84, no. 8,pp.563-575, 2005.

[66] M. Srinivasan, "Energetics of legged locomotion: Why is total metabolic cost proportional to the cost of stance work," *Proc. on ISB XXth Congress and the American Society of Biomechanics Annual Meeting,* Cleveland, Ohio, pp. 829, August 2003.

[67] J. Doke, J. M. Donelan, and A. D. Kuo, "Mechanics and energetics of swinging the human leg," *The Journal of Experimental Biology,* No. 208, pp.439-445, 2005.

[68] R. Riener, M. Rabuffetti, and C. Frigo,"Stair ascent and descent at different inclinations," *Gait Posture,* Vol. 15, pp. 32-44, 2002.

[69] B. J. McFadyen and D. A. Winter, "An integrated biomechanical analysis of normal stair ascent and descent," *Journal of Biomech,* Vol. 21, No. 9, pp. 733-44, 1988.